Mon. Not. R. Astron. Soc. **262,** 764–794 (1993)

Evidence for systematic evolution in the properties of galaxies in distant clusters

Alfonso Aragón-Salamanca,[1] Richard S. Ellis,[1] Warrick J. Couch[2] and David Carter[3]

[1]*Physics Department, University of Durham, South Road, Durham DH1 3LE*
[2]*School of Physics, University of New South Wales, Kensington, NSW, Australia*
[3]*Royal Greenwich Observatory, Madingley Road, Cambridge CB3 0EZ*

Accepted 1992 November 30. Received 1992 November 27; in original form 1992 August 19

ABSTRACT

This paper investigates the evolution of galaxies as a function of look-back time, primarily using early-type galaxies in rich cluster environments. We demonstrate that, by selecting distant galaxies in the near-infrared, representative samples containing approximately the same proportion of galaxy classes can be constructed independently of redshift, thus avoiding biases introduced by optical selection criteria. Using this method, we construct a sample of 180 galaxies selected at near-infrared wavelengths in the fields of 10 rich clusters with $0.5 < z < 0.9$. Observing and data processing techniques, with infrared arrays yielding the required high-precision photometry of cluster members, are discussed. Additional optical CCD photometry allows us to quantify colour evolution as a function of redshift for the early-type members to $z \sim 1$. We detect a clear and systematic trend with redshift in the optical–infrared colours of *red* cluster galaxies. Specifically, by $z \sim 0.9$ there are *no* cluster galaxies as red as present-day ellipticals. The detected evolution is monotonic with redshift and consistent with the passive ageing of stellar populations formed before $z \approx 2$. Moreover, the uniformity in these trends among our clusters suggests that early-type galaxies are coeval and form a remarkably homogeneous population. The evolution we find is both more well-behaved and less prominent than that found for powerful radio galaxies, suggesting that the latter sources may not be representative giant elliptical galaxies.

Key words: galaxies: active – galaxies: evolution – galaxies: formation – galaxies: photometry – cosmology: observations – infrared: galaxies.

1 INTRODUCTION

A major goal in observational cosmology is the measurement of detailed changes in the integrated spectral energy distributions of normal galaxies as a function of look-back time. Such changes are predicted by stellar evolution, and to quantify them as a function of redshift would constrain the ages of galaxies, their star formation histories and possibly the cosmological model. Surprisingly little is known observationally about how galaxies came to be in their present state. At the most fundamental level, it remains unclear whether galaxies are in any sense *coeval*, sharing a similar evolutionary history, or whether stars formed over a wide range of epochs, even for systems that have remarkably similar properties today.

Measurement of the evolution of galaxies for the purposes outlined above can be approached observationally in several ways, assisted by evolutionary models constructed by e.g. Tinsley (1972), Bruzual (1983), Arimoto & Yoshii (1986, 1987) and Charlot & Bruzual (1991). Most work has concentrated on two specific methods. First, one can establish large samples of faint field galaxies selected photometrically and, by linking changes in the distributions of broad-band colour and luminosity with redshift, determine the gross evolutionary behaviour of what are unbiased samples. The approach is well documented (e.g. Bruzual & Kron 1980; Koo 1986), and a large body of reliable spectroscopic data has been gathered in recent years which adds the crucial redshift baseline to the earlier photometric methods (see Ellis 1990 for a review).

Two complications arise, however, that make this method unattractive as the principal observational approach to the understanding of galaxy evolution. First, the field contains a diverse population of galaxies and it is not straightforward to connect populations at one redshift with their predecessors at higher redshift without making dubious assumptions about the history of star formation for given classes. Since a star-forming blue galaxy can become optically red and dim relatively quickly (1–2 Gyr) or return to being blue and luminous even more rapidly, the diversity in colour at any one epoch implies that many evolutionary solutions may simultaneously explain even a large body of excellent data taken from the field.

The second complication is more fundamental, but at the same time puzzling. At the current spectroscopic limits of 4-m telescopes ($B \simeq 24$), few field galaxies are found at large look-back times; indeed, a high proportion of the faintest sources have redshifts $z \leq 0.3$ (Colless et al. 1990, 1993; Cowie, Songaila & Hu 1991). Quite apart from the inefficiency of finding galaxies at large look-back times, the rapid evolution in *numbers* implied by the high counts which probe to unexpectedly modest depths reinforces the complications discussed above. At the present time, only widespread merging since $z \simeq 1$ or a population of blue dwarf galaxies that has disappeared by the present epoch appears to satisfy the current data sets (Broadhurst, Ellis & Glazebrook 1992). Although it is important to understand this conundrum, such added complications are hardly conducive to the determination of unique evolutionary solutions.

The alternative approach is to examine a uniform subset of the galaxy population which can be identified over a wide range in redshift. Early-type galaxies in rich clusters are the obvious choice. There is good evidence for the homogeneity of the population in nearby clusters (Bower, Lucey & Ellis 1992a,b) and, logically, these systems are the natural stepping-stone into galaxy evolution from the well-studied globular clusters in the Galaxy. Clusters of galaxies have been identified to very high redshifts and thus, by examining well-defined populations of cluster galaxies at various redshifts, galaxy evolution can perhaps be quantified more readily, albeit for a restricted class of galaxy.

This approach has been pursued photometrically by Butcher & Oemler (1978, 1984), Couch et al. (1983) and Couch & Newell (1984). These authors found little evidence for evolution in the colours of the dominant *red* cluster population to $z \simeq 0.5$, but identified an increasing fraction of blue luminous members (the 'Butcher–Oemler effect') whose origin has been the subject of much attention. Spectroscopic surveys (Dressler & Gunn 1982; Dressler, Gunn & Schneider 1985; Lavery & Henry 1986; Couch & Sharples 1987) and further photometric work (MacLaren, Ellis & Couch 1988) suggested that a subset of cluster galaxies may suffer short-term bursts of star formation arising from dynamical processes within the clusters (for a recent review, see Oemler 1992). An important clue is the claim that the blue galaxies avoid the central regions of the cluster (Butcher & Oemler 1984; Schneider, Dressler & Gunn 1986), although no strong dynamical distinction is yet apparent (Allington-Smith et al. 1993). The picture emerging is that of a 'red envelope' in the rest-frame colour–luminosity plane (cf. O'Connell 1988) populated by early-type galaxies drawn mostly from the cluster core, whose spectral properties remain largely unchanged to $z \simeq 0.5$, together with an evolving population of bluer star-forming galaxies whose cause and underlying morphological nature remain unclear.

To what redshift does this 'red envelope' remain unchanged? Beyond $z \simeq 0.5$, little photometric information has been published for normal cluster galaxies, although the two major surveys of distant clusters (Gunn, Hoessel & Oke 1986; Couch et al. 1991) have identified systems to $z \simeq 0.9$. In a pioneering study, Hamilton (1985) found that intrinsically red galaxies exist to $z \simeq 0.8$ and suggested that the early-type population could be very old, as already indicated by the models of Tinsley & Gunn (1976). However, his sample was small (only four galaxies were found beyond $z = 0.6$) and could not therefore test the basic *coevality* assumption. Coevality could be checked by examining how representative Hamilton's galaxies are with respect to a larger sample at the same epoch, e.g. drawn from a variety of environments.

The purpose of this paper is to report a new extensive study, based on the spirit of Hamilton's approach but extending his analysis to over 100 faint galaxies selected from 10 rich clusters with $0.54 \leq z \leq 0.92$. The principal aim is to track evolution in the 'red envelope' of the cluster colour–luminosity diagram, as well as to examine the relationship between any such trends and the Butcher–Oemler effect to redshifts much larger than hitherto addressed. The distinction is important, because early-type galaxies cannot be selected morphologically beyond $z \simeq 0.2$. By selecting distant galaxies via their optical luminosities and colours we may, unwittingly, discover galaxies undergoing short-term star formation and confuse two distinct processes. This criticism could apply to the claim by Dressler & Gunn (1990) for significant spectral evolution in the reddest objects in their distant clusters with $z > 0.7$. Our second major advance in this work, which addresses this problem, is our use of *infrared imaging* to select cluster galaxies. We demonstrate that only by selecting galaxies in the K band ($\lambda_{\rm eff} \equiv 2\ \mu$m) can samples unaffected by most kinds of star formation activity be constructed. Together with optical photometry, the two forms of evolution can effectively be distinguished.

Our photometric samples are more complete and considerably deeper than can be secured spectroscopically; thus we have adopted a statistical approach, accounting for background and foreground contamination via published deep field photometry in a manner similar to that originally used by Butcher & Oemler. However, we demonstrate, using a subset of clusters with more detailed spectroscopic and spectrophotometric information, that this is a reliable process.

Our study complements, in an important way, a parallel effort to secure the detailed optical–infrared spectrophotometry of large samples of distant *radio* galaxies extending to much higher redshifts ($z \simeq 4$) (Lilly & Longair 1984; Djorgovski, Spinrad & Maar 1985; Lilly 1988, 1989a; Chambers & Charlot 1990). While many local radio sources are found in luminous elliptical galaxies, the connection is not yet physically understood and, indeed, the interpretation of their optical–infrared radiation in terms of normal stellar evolutionary processes remains controversial (cf. Scarrott, Rolph & Tadhunter 1990). By comparing any evolutionary trends found from our sample of distant cluster galaxies with that delineated from extensive work on distant radio galaxies, we may be able to verify whether distant radio galaxies are

evolving physically in a similar way to early-type cluster galaxies.

A plan of the paper follows. In Section 2 we describe our observational approach, justifying the need to select galaxies in the near-infrared and describing our cluster sample. In Section 3 we present the data, the observing techniques and reduction procedures used to build the optical and infrared photometric catalogues. Section 4 presents our photometric results in terms of colour–magnitude and colour–colour diagrams, comparing these with appropriately constructed plots for nearby clusters. We then discuss the field contamination and examine colour evolution as a function of redshift. The measured evolution is compared with the predictions of galaxy evolution models distinguishing between gradual monotonic evolution of the early-type component (the red envelope) and a declining fraction of blue cluster galaxies. Section 5 discusses the K-band luminosity evolution in the context of that identified for distant radio sources. In Section 6 we present the conclusions of the paper.

2 OBSERVATIONAL APPROACH

The principal method we adopt is to select samples of cluster galaxies in the K band, using their optical–IR colours to monitor changes in the spectral energy distributions (SEDs) and thereby their early star formation histories. Optical photometry at $z > 0.5$ samples rest-frame UV light that should be sensitive to even small amounts of star formation. Evolutionary changes can be measured by comparing precision *VIK* photometry for cluster galaxies with $0.5 \lesssim z \lesssim 0.9$ with similar observations for nearby clusters. Since the local samples have more extensive colour data (e.g. *UBVRIJK*), we can make colour comparisons in rest-frame bands that are closest to those observed at high redshift, hence bypassing much of the uncertainty involved in applying redshift or k-corrections.

Spectroscopic redshifts are not available for most of the galaxies selected in our deep K-band images, so cluster members must be defined statistically by subtracting appropriately scaled colour distributions for field galaxies from published number counts (Cowie et al. 1990; Lilly, Cowie & Gardner 1991; Cowie et al. 1992). Two clusters, 0016+16 and F1767.10TC, for which spectroscopic information is available, provide a realistic test of the conclusions derived using this statistical approach.

The amount of evolution detected can be interpreted using Bruzual's (1983) models of galaxy evolution to constrain the age and history of star formation in *normal* cluster galaxies. Two questions are paramount. Are the evolutionary trends seen similar from cluster to cluster at a given redshift, such as might be expected if early-type galaxies are coeval? Secondly, what constraints can we place on the epoch of major star formation in these galaxies?

2.1 Infrared versus optical selection

When trying to understand the evolution of galaxies with look-back time, we need to build samples that are representative of the galaxy population at different redshifts, i.e. we have to select galaxies in a way that does not depend on the evolutionary effects that we are trying to detect. Ideally, we would like to have a sample that contains the same proportion of galaxy types at all redshifts. Two biases are particularly important in this respect. First, whereas the SEDs of present-day galaxies of different types are similar at near-infrared wavelengths, there are large differences in the ultraviolet which imply very different k-corrections for any high-redshift observations made at optical wavelengths. *Even without evolution, an optically selected sample would be biased towards UV-bright late-type galaxies at higher redshifts, distorting the mixture and generating a false evolutionary trend.* Secondly, if evolution is present, this will tend to select preferentially the UV-strong galaxies, making quantitative conclusions difficult to draw. Whilst optical studies do bring evolving sources into view, it is the *proportion* of the population that shares this evolution that it is crucial to understand. To overcome these problems, which we will refer to as the *ultraviolet bias*, is critical to any reliable measurement of galaxy evolution.

However, because the SEDs are more uniform in the near-infrared, infrared k-corrections for the redshift range $z < 1$ are virtually independent of Hubble class (Elston 1991). A uniform mixture of galaxy types is therefore maintained for K-limited cluster samples over a wide range in redshift (Aragón-Salamanca et al. 1993). Furthermore, if evolution occurs, for example, via an enhanced star formation rate, the source detection probability will be largely unaffected at long wavelengths.

To demonstrate the importance of the bias introduced by the optical selection of galaxies at high redshift, we have taken the optical–infrared colour–magnitude data for the cluster Abell 370 ($z = 0.37$, Aragón-Salamanca, Ellis & Sharples 1991, hereafter AES) and systematically 'moved' the cluster to higher redshifts, contrasting colour distributions formed from r- and K-selected samples. The $(685-K)$ colours of AES were transformed into $(r-K)$ using AES's 685-to-R calibration and Schneider, Gunn & Hoessel's (1983a) r-to-R transformation. Fig. 1 shows the resulting $(r-K)$ versus K diagram for Abell 370 as viewed at a variety of redshifts. The areas above the lines marked 'r = 23' indicate those regions in colour–luminosity space that would be lost at high redshift when using an $r \sim 23$ limit similar to that appropriate in a spectroscopically constructed sample of cluster galaxies (cf. Dressler & Gunn 1990, 1992 – see Section 4.2.6). Representative K limits from the present survey are indicated: these vary slightly from cluster to cluster within our sample. As expected, the colour distributions for K-selected samples are uniformly depopulated as redshift increases, but those for r-selected samples preferentially lose the red members, *thereby producing a false evolutionary trend*. The magnitude of this bias would, of course, be lessened if colour evolution were present (in the case of strong evolution where all sources get bluer, it might be quite negligible), but there is no way from optical data alone to determine how serious a problem this might be.

2.2 The cluster sample

Few galaxy clusters with $z \gtrsim 0.5$ are known, and virtually all have been found in the photographic F ($\lambda_{\rm eff} \sim 6100$ Å) and N ($\lambda_{\rm eff} \sim 8000$ Å) bands. Those for the present study were taken from two optical surveys specifically designed to find high-redshift clusters, namely the catalogues of Gunn et al.

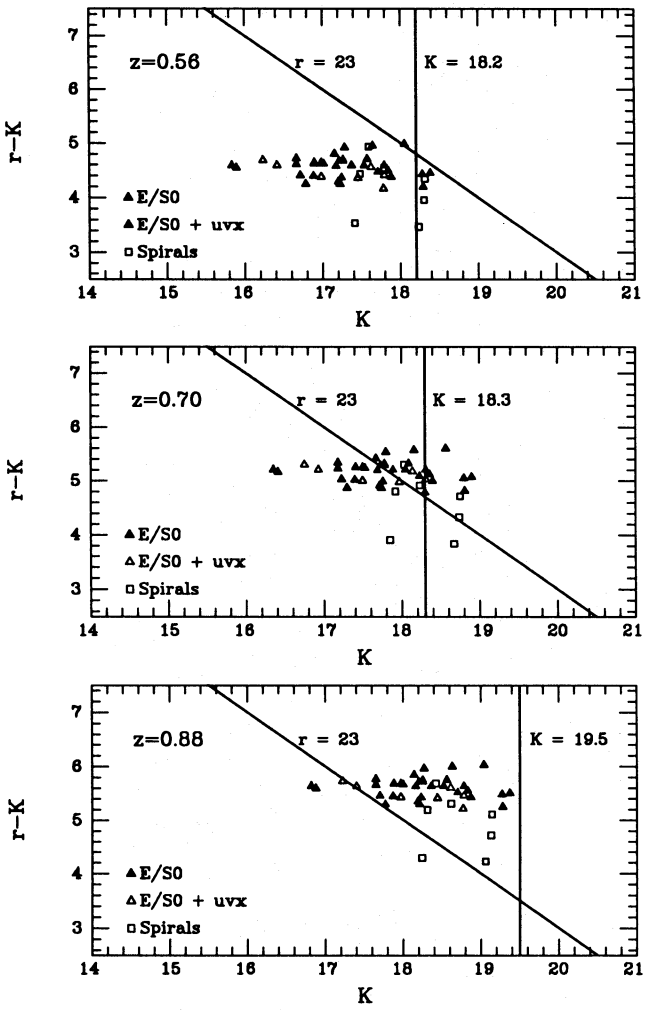

Figure 1. $(r-K)$ versus K C–M diagrams for model clusters at different redshifts, based on the data for Abell 370 (see text). The vertical lines show the limits of a K-selected sample at different limiting magnitudes (representative of our data). The inclined lines show the limits of an r-selected sample with $r<23$.

(1986, hereafter GHO) and Couch et al. (1991, hereafter CEMM). The sample is presented in Table 1.

GHO's clusters were found on Mayall 4-m F and N prime-focus plates and Hale 5-m prime-focus image intensifier exposures recorded on photographic plates (approximately N band). The precise selection criteria are not well documented. Redshifts have been published for 25 clusters, of which eight have $z \geq 0.55$, and seven are included here. We discarded Cl1322+3115 ($z=0.755$) because a visual inspection of GHO's images indicated it to be somewhat less rich than their other examples at a similar redshift. We included Cl1603+4329 ($z=0.920$) despite worries that it may be the superposition of two clusters at redshifts $z=0.90$ and 0.94 (Dressler & Gunn 1990). For the purpose of studying galaxy evolution, the redshift difference between the clusters makes very little difference, even though they might be two separated dynamical entities.

CEMM identified clusters on high-contrast film derivatives of AAT 3.9-m prime-focus plates taken in the J and F passbands according to their contrast, σ_{cl}, above the fluctuations in the field counts as determined locally on the same fields. They claimed that their cluster list should be complete above a limit of $\sigma_{cl}=3.25$. Again, a large fraction of the clusters have no redshifts, although a subsample with $\sigma_{cl} \geq 4$ is complete. Three CEMM clusters have $z \geq 0.55$, but one (J1836.23TR, $z=0.68$) was discarded, since spectra for nine objects were required to secure two with the same redshift. A tenth optically selected cluster, 0016+16 ($z=0.54$: Spinrad 1980; Koo 1981; Ellis et al. 1985; Aragón-Salamanca 1991, and references therein), was added to the sample from outside these catalogues in view of the large body of optical photometry and spectroscopy available. Fig. 2 shows the redshift distribution of the galaxy clusters.

Table 1. Cluster sample.

Cluster	Redshift	References
0016+16	0.546	(1,2)
J1888.16CL*	0.563	(3,4)
Cl0317+1521	0.583	(5)
F1767.10TC	0.664	(4)
Cl1322+3029	0.697	(5)
Cl0020+0407	0.698	(5)
Cl1322+3027	0.751	(5)
Cl2155+0334	0.820	(5)
Cl1603+4313	0.895	(5)
Cl1603+4329	0.920	(5)

*Also known as F2262.16CL and 0055 − 279.

References: (1) Spinrad (1980); (2) Koo (1981); (3) Couch et al. (1985); (4) Couch et al. (1991); (5) Gunn et al. (1986).

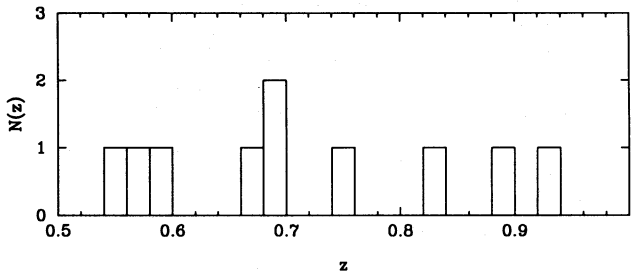

Figure 2. Redshift distribution of the cluster sample.

Selection effects clearly play an important role in optically selected catalogues of distant clusters (see the extensive discussion in CEMM). Redshift-dependent selection effects can be reduced by using progressively redder bands for more distant samples, and superposition difficulties can be addressed with multiple-object spectroscopy. The *galaxy-dependent* selection effects associated with variations in stellar populations at a given epoch are clearly the most important in the present study. Our main aim is to study the properties of the cluster *galaxies* as a function of redshift, not the *clusters* themselves, which simply provide convenient samples with a common z (and possibly a common star formation history) in small areas of sky. While cluster-

dependent biases are inevitably present in Table 1, the critical question is whether such biases are transferred to the constituent galaxies. For example, might there be clusters dominated by very red or very blue sources missed by GHO or CEMM? We cannot address this possibility carefully until an independently produced survey of distant clusters, e.g. using X-ray selection, becomes available. However, we note that the volume densities derived by these authors for optically selected rich clusters at $z \simeq 0.5$ are consistent with those observed today, indicating that no sizeable loss of the precursors of present-day clusters has occurred. Additionally, CEMM were able to contrast, very effectively, the visibility of some of their distant clusters as seen on both the *J* and *F* films. While many clusters were more prominent on the *J* films, this was attributed to the effects of star formation in a subset of the members: the same clusters were readily detected on their *F* films.

3 DATA

3.1 Infrared data

K-band photometry for our sample of high-redshift clusters was obtained using IRCAM at the 3.8-m UK Infrared Telescope (UKIRT) during 1989–91. IRCAM is a 1–5 μm imager based on a 62 × 58 InSb array offering a range of pixel scales (McLean et al. 1986). The 1.24-arcsec pixel mode was used in all cases except for Cl1603+4329, where we used 0.62-arcsec pixels; Table 2 presents a log of the IR observations.

The observing and data reduction procedures followed those of AES (see also Aragón-Salamanca 1991), and we review these briefly here. On-chip exposures were chosen to give background-limited operation (typically 8–15 s in the 1.2 arcsec pixel^{-1} configuration), and ~25 such exposures were combined to form a single 'co-added frame'. A slight non-linearity of the array response has been calibrated by M. Casali (private communication), and is found to be stable with time. We thus applied a small correction factor to the counts in each pixel of the raw images to allow for this prior to any reduction. A dark current was first subtracted using the closest of several DARK frames taken every few hours. A high-quality flat-field, SKYFLAT, was obtained by combining several images taken in blank areas of the sky near the target, generally with the same on-chip exposure and number of co-adds as the object frames. Significant variations have been found in the SKYFLAT images on time-scales as short as 10–15 min, and flat-fielding is often affected by offsets of as little as a few degrees. Unfortunately, to ensure the maximum signal-to-noise ratio we found it necessary to spend as much time on SKYFLATS as on the cluster targets, nodding the telescope between each every ~10 min. Each individual target and sky frame was taken at a slightly different position ('dithered') in order to minimize residual pixel-to-pixel variations in sensitivity, the effects of bad pixels and cosmic rays, and the effect of faint stars in the sky images.

The combined SKYFLAT was normalized to unity and used as a conventional flat-field for the science exposures. In practice, the best results are obtained by restricting the combination to those sky images taken immediately before and after each target image. Building of a 'super-flat' by median-filtering all the sky exposures over a long period produces inferior results because of the rapidly changing nature of the detector response. After flat-fielding, known artefacts (e.g. bad pixels) were replaced by interpolation between adjacent pixels, the target images were registered using measured subpixel shifts and the median of all suitable exposures used to produce a final image. Since the field of view of the camera is quite small, it was necessary in some cases to image the targets at different positions to obtain a mosaic.

Very flat images (flatter than 7 parts in 10^5 in exposure times of $\simeq$5000 s) have been obtained using the offset-sky method described above, corresponding to a 1 σ surface brightness detection limit of ~22.8 mag arcsec^{-2}. Although impressive results have also been obtained by the 'in-field' flat-fielding technique discussed by Cowie et al. (1990) and Smail et al. (1993), which does not require extensive off-target exposures, that alternative cannot be used here because the cluster fields are too crowded and the galaxies are often too faint to be seen in exposures as short as the optimum ones, making the registration of the images very difficult.

Absolute photometric calibration was obtained via frequent observation of standard stars from Elias et al. (1982). Typical uncertainties on the zero-points are ~0.02–0.03 mag. Although a small fraction of the observations were carried out in non-photometric conditions, in every case enough photometric data were obtained for each cluster to ensure absolute calibration with the required precision.

Aperture photometry was obtained using circular apertures centred on each object, with local sky estimated from the mode inside similar apertures in carefully chosen adjacent blank areas. A 4.8 arcsec diameter aperture was used in most cases; this is optimal for maximization of the fraction of the total light inside the aperture while avoiding crowding effects. For F1767.10TC and Cl1322+3029, the *K* images were obtained before the image quality of the telescope and camera was substantially improved, and for C12155+0334 the seeing in the associated optical data was ~2.5 arcsec. For these cases, the inferior image quality forced us to use a 6.4 arcsec diameter aperture. Random photometric errors were estimated using the sky variance, and by direct comparisons between repeat measures and those on overlapping areas. Both estimates gave similar results, even across different observing runs. For most of the objects, we have more than one independent measurement and the final *K* magnitude was computed as the inverse-variance weighted mean. For each cluster, a photometric catalogue was constructed to a limit at which the photometric errors were $\simeq$0.2 mag (5 σ). These *K*-magnitude limits vary slightly from cluster to cluster (for example, the most distant cases were deliberately subjected to deeper exposures) and are summarized in Table 2.

Contour maps of the final *K* images are shown in Fig. 3 and the catalogued objects are identified. For 0016+16, only the central portion of a mosaic of four images is shown.

3.2 Optical photometry

Optical CCD images in the *V* and Kron–Cousins *I* bands were obtained for our cluster sample, mostly in service exposures at the 4.2-m William Herschel and 3.9-m Anglo–Australian telescopes during 1989–91. The only exceptions

Table 2. Log of the *K*-band observations.

Cluster	R.A. (1950)	Dec. (1950)	Date	Camera	Exp. t (s)
0016+16 (1)	$00^h15^m57^s.0$	+16°09′06″	1988 Oct 13/14	IRCAM I	6000
			1988 Oct 16/17	IRCAM I	3000*
(2)	$00^h15^m57^s.0$	+16°10′14″	1988 Octr 13/14	IRCAM I	3000
			1988 Oct 15/16	IRCAM I	3000*
(4)	$00^h15^m57^s.0$	+16°09′37″	1989 Oct 3/4	IRCAM II	4000
(NE)	$00^h16^m01^s.4$	+16°10′14″	1990 Jul 20/21	IRCAM II	1600
(NW)	$00^h15^m54^s.2$	+16°09′39″	1990 Jul 21/22	IRCAM II	1440
(SE)	$00^h16^m03^s.0$	+16°09′10″	1990 Jul 22/23	IRCAM II	1440
J1888.16CL	$00^h54^m31^s.6$	−27°56′43″	1989 Oct 4/5	IRCAM II	2600
			1989 Oct 5/6	IRCAM II	2000
Cl0317+1521	$03^h17^m14^s.5$	+15°21′00″	1989 Oct 3/4	IRCAM II	6250
			1989 Oct 4/5	IRCAM II	600
F1767.10TC	$08^h44^m53^s.4$	+18°04′09″	1989 Apr 10/11	IRCAM I	9000
			1989 Apr 11/12	IRCAM I	6000*
Cl1322+3029	$13^h22^m00^s.7$	+30°28′39″	1989 Apr 9/10	IRCAM I	9000*
			1989 Apr 10/11	IRCAM I	6000
Cl0020+0407	$00^h20^m18^s.0$	+04°07′49″	1989 Oct 3/4	IRCAM II	4000
			1989 Oct 4/5	IRCAM II	2400
			1989 Oct 5/6	IRCAM II	1800
Cl1322+3027	$13^h22^m28^s.4$	+30°27′10″	1990 Jul 18/19	IRCAM II	2000*
			1990 Jul 20/21	IRCAM II	1200
Cl2155+0334	$21^h55^m23^s.8$	+03°33′31″	1990 Jul 17/18	IRCAM II	5200
			1990 Jul 18/19	IRCAM II	4400*
			1990 Jul 19/20	IRCAM II	5600*
			1990 Jul 22/23	IRCAM II	2400
Cl1603+4313	$16^h02^m46^s.1$	+43°13′00″	1990 Jul 18/19	IRCAM II	2000*
			1990 Jul 19/20	IRCAM II	800*
			1990 Jul 20/21	IRCAM II	4800
			1990 Jul 21/22	IRCAM II	8160
			1990 Jul 22/23	IRCAM II	4800
Cl1603+4329 (S)	$16^h02^m53^s.4$	+43°29′20″	1991 Aug 10/11	IRCAM I	1920†
			1991 Aug 11/12	IRCAM I	3200†
(N)	$16^h02^m53^s.8$	+43°29′46″	1991 Aug 12/13	IRCAM I	3200†
			1991 Aug 13/14	IRCAM I	3200†

*Non-photometric; †0.62 arcsec pixel^{-1} scale.

are the images of J1888.16CL (≡F2262.16CL or 0055−279), for which the original images used by Couch, Shanks & Pence (1985) were supplied, and 0016+16 and Cl1603+4313, for which images obtained by Smail et al. (in preparation) as part of a deep search for gravitationally lensed images were used. Table 3 summarizes the log of the optical observations.

The optical images were reduced in a standard way. Occasional large-scale flat-fielding residuals remained due to the imperfect matching of the flat-field source used and the night sky. This problem was overcome by producing a median 'super-flat' using all the deep images taken in the same filter during that night. Using this flat-field, the large-scale variations were reduced to a level comparable to the pixel-to-pixel variations on the sky. The images taken using an RCA-CCD presented some fringes, especially in the *I* band. These were removed by subtracting suitably scaled fringe frames taken of blank fields.

Absolute photometric calibration was provided by the analysis of images of Landolt (1983) and Graham (1982)

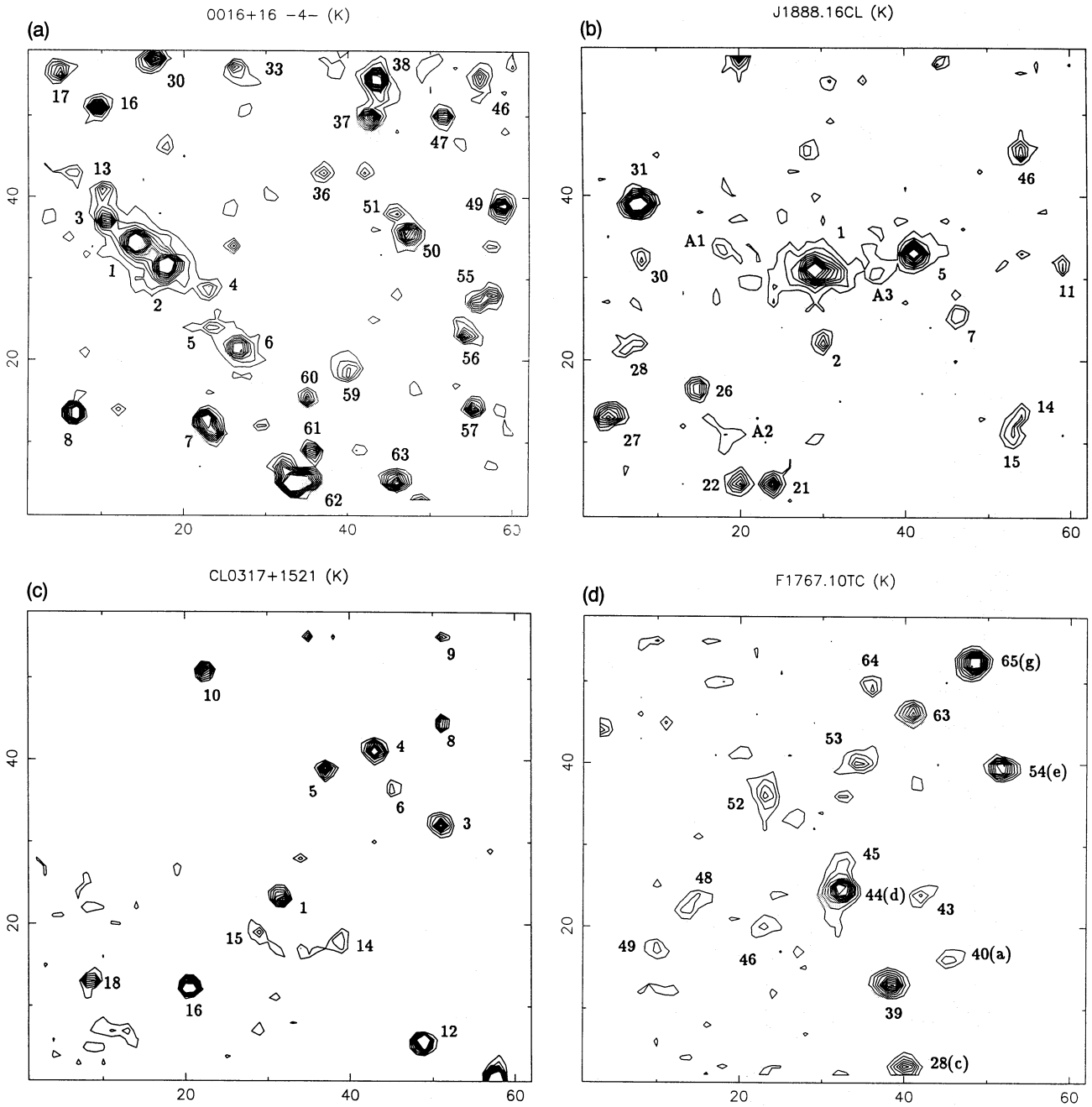

Figure 3. (a) Contour plot of the 0016+16 (central region) *K*-band image. The scale is 1.24 arcsec pixel^{-1}. The numbers on the axes are pixels. North is up and east is to the left. The contours follow a linear intensity scale, the lowest corresponding to 2 σ above average sky level and the highest to 20 σ. (b) As (a), for J1888.16CL (also known as F2262.16CL or 0055−279). (c) As (a), for Cl0317+1521. (d) As (a), for F1767.10TC. (e) As (a), for Cl1322+3029. (f) As (a), for Cl0020+0407. (g) As (a), for Cl1322+3027. (h) As (a), for Cl2155+0334. (i) As (a), for Cl1603+4313. (j) As (a), for Cl1603+4329, but with a pixel scale of 0.62 arcsec pixel^{-1}. The image is a mosaic of two frames.

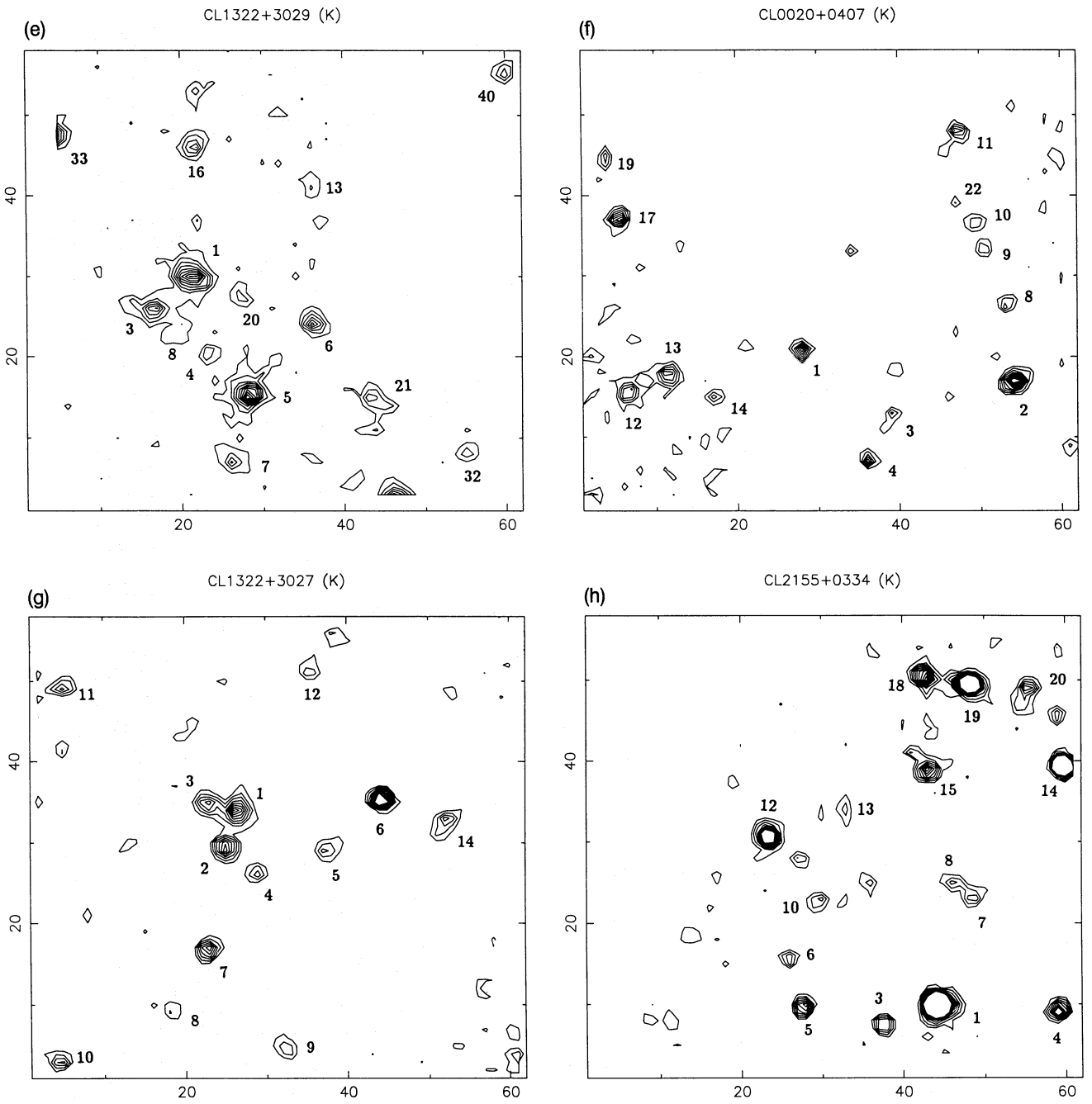

Figure 3 – *continued*

standard stars that yielded zero-point errors of $\lesssim 0.02$ mag. Photometry was performed using apertures that match those used in the IR. Similar error analysis to that described in Section 3.1 yielded the internal photometric errors presented in Table 4. The use of different telescopes, instruments and CCD detectors has led to cluster photometry in slightly different photometric systems. In V the differences are negligible, but in I some colour terms remain. Using present-day SEDs for galaxies of different types, we can estimate the size of this effect. The effect of the variations in the I response increases for redder objects, reaching ~ 0.1 mag in $(I-K)$ for an elliptical at $z=0.9$; in $(V-I)$ the maximum change is ~ 0.07 mag. We chose not to correct for these colour terms because the standard stars used do not span a wide enough colour range. Instead, we have used the appropriate filter + detector response curve in every case when computing the non-evolutionary predictions with which the data are compared. Further details are given in Section 4.1.1.

The optical and IR data were gathered under different seeing conditions (Tables 2 and 3), and a correction was applied to the aperture magnitudes and colours following the method described by Bower et al. (1992a). The correction is only very weakly dependent on the size of the model galaxy used to compute it, and an effective radius of $r_e = 0.5$ arcsec was used for all galaxies. The average corrections were 0.12 mag for the K magnitudes and 0.06 mag in V and I, so that

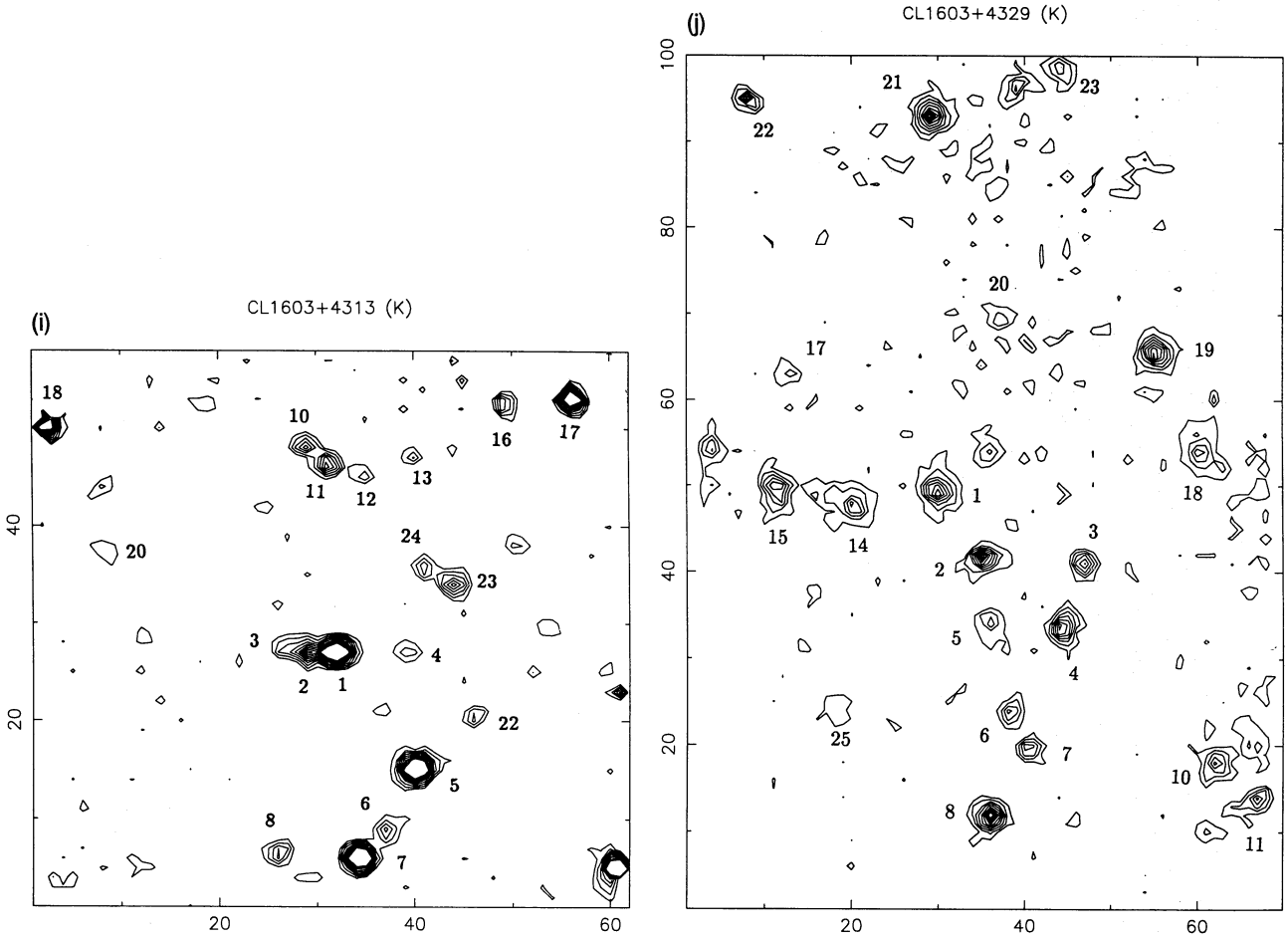

Figure 3 – *continued*

the corrected optical–IR colours are, on average, 0.06 mag redder than the measured ones. The uncertainty introduced by this correction is negligible compared with other sources of random error.

3.3 Photometric catalogue

The final K magnitudes, VIK colours and adopted internal 1σ errors are given for each cluster in turn in Tables 4(a) to (j). The numbering scheme refers to that in Fig. 3, with the exception of the two lower redshift clusters for which extensive analyses have already been carried out. For 0016+16 we adopt the numbering scheme of Ellis et al. (1985), except for a few objects that were not present in their sample. For those we use the identifications of Dressler & Gunn (1992) prefaced with a 'D'. For J1888.16CL we adopt the numbering scheme of Couch et al. (1985), adding four objects (A1–A4) seen in K but not present in their optical catalogue.

Two clusters have been studied spectroscopically and spectrophotometrically in further detail. For 0016+16 we tabulate photometric redshifts and spectral classifications based on intermediate-band CCD photometry from the survey of Ellis et al. (1985), as well as available spectroscopic information from Dressler & Gunn (1992). Hitherto unpublished multiband data are also available for F1767.10TC which has been used in a similar way, and spectroscopic redshifts are available from CEMM.

Contamination from stars can be expected, depending on Galactic latitude. Fig. 4 shows the position of Galactic stars on the $(V-I)$ versus $(I-K)$ plane (Johnson 1966; Koornneef 1983; Cowie et al. 1992), together with the expected loci of galaxies of different spectral types at different redshifts (derived from the SEDs used to make the non-evolutionary prediction). In this colour–colour plane, stars are well separated from galaxies regardless of their nature and redshift, and we have thus used our colours as an aid to image classification. Since most of the optical images have good seeing (see Table 3), we can check this procedure independently. We find that the colour and image classifications are in excellent one-to-one agreement. The objects we have classified as stars are denoted by an asterisk on the tables, and are excluded from further analyses.

Our catalogue presents K-limited photometry for a total of 180 galaxies in 10 high-z clusters: ~18 per cluster. Photometric errors in K are always $\lesssim 0.2$ mag. While the optical photometric precision depends on the colours of the objects and the optical exposure times, in most cases this is comparable to or better than that in K, except for a few very red objects (see Table 4). In five cases, a K-detected object was not seen in the V band. For these, $\sim 3\sigma$ lower limits on the colours are given in the tables. Since these objects are very few in number, they will not significantly affect our conclusions, but we will take these limits into account when necessary.

Table 3. Log of the optical observations.

Cluster	Telescope	Instrument	Detector	Scale (″/*pixel*)	Date	Seeing	Band	Exposure (s)
0016+16	4.2 m WHT	Taurus II (f/4)	GEC–EEV (800 × 1180)	0.27	1990 Jul 21/22	0.″9	*V*	11000
	"	"	"	"	1990 Jul 23/24	1.″1	*I*	10000
J1888.16CL	3.9 m AAT	Prime Focus (f/3.3)	RCA (320 × 512)	0.49	1982 Aug 27/28	1.″2	*V*	800
	"	"	"	"	"	1.″2	*I*	800
Cl0317+1521	4.2 m WHT	Taurus II (f/4)	GEC–EEV (800 × 1180)	0.27	1990 Sep 11/12	1.″1	*V*	2000
	"	"	"	"	"	1.″1	*I*	1200
F1767.10TC	3.9 m AAT	Prime Focus (f/3.3)	RCA (320 × 512)	0.49	1985 Dec 13/14	1.″8	*V*	2420
	"	"	"	"	1986 Mar 12/13	2.″0	*V*	500
	"	"	"	"	1985 Dec 13/14	1.″7	*I*	2000
Cl1322+3029	4.2 m WHT	Taurus II (f/4)	GEC (385 × 578)	0.27	1989 Jun 26/27	0.″8	*V*	2400
	"	"	"	"	1989 Mar 28/29	0.″9	*I*	1200
Cl0020+0407	3.9 m AAT	Prime Focus (f/3.3)	RCA (320 × 512)	0.49	1990 Jun 22/23	1.″2	*V*	2000
	"	Prime Focus (f/2)	Thompson (1024 × 1024)	0.50	1989 July 7/8	1.″0	*I*	1000
Cl1322+3027	4.2 m WHT	Taurus II (f/4)	GEC (385 × 578)	0.27	1989 Jun 26/27	0.″8	*V*	2400
	"	"	"	"	1989 Mar 28/29	0.″9	*I*	1200
Cl2155+0334	3.9 m AAT	Prime Focus (f/3.3)	RCA (320 × 512)	0.49	1990 Jun 21/22	2.″5	*V*	2000
	"	"	"	"	"	2.″5	*I*	1000
Cl1603+4313	4.2 m WHT	Taurus II (f/4)	GEC–EEV (800 × 1180)	0.27	1990 July 21/22	0.″8	*V*	8000
	"	"	"	"	1989 July 23/24	0.″9	*I*	12000
Cl1603+4329	2.5 m INT	Prime Focus (f/3)	GEC (385 × 578)	0.54	1991 July 11/12	0.″9	*V*	4000
	"	"	"	"	"	0.″9	*I*	3500

Table 4. (a) 0016 + 16: aperture = 4.8 arcsec; $K \lesssim 18.2$ mag.

#	K	σ_K^*	$(V-I)^*$	$(V-K)^*$	$(I-K)^*$	$\sim z^\dagger$	Class†	Spectroscopy‡
62	15.42	0.02	1.91	4.89	2.98	0.3	E/S0	0.301
2	15.78	0.03	2.44	5.59	3.15	0.55	E/S0	0.543 Early
1	15.80	0.03	2.40	5.54	3.14	0.55	E/S0	0.532 Early
7	16.17	0.03	2.76	5.80	3.04	0.55	E/S0	0.540
38	16.35	0.03	2.28	5.38	3.10	0.3–0.4	Sab	0.654
*8	16.47	0.05	1.93	3.80	1.87	—	—	0.000 K star
6	16.50	0.05	2.56	5.45	2.89	0.6–0.7	E/S0	0.539 Poor s/n
63	16.61	0.05	1.82	4.64	2.82	0.4–0.6	Scd	0.546 [OII]
144	16.62	0.06	2.09	4.95	2.86	0.3	Sab	0.560 PSG
49	16.65	0.05	2.51	5.43	2.92	0.3	E/S0	—
3	16.68	0.07	2.37	5.61	3.24	0.55	Sab	0.541 Early
50	16.69	0.04	2.54	5.50	2.96	0.55	E/S0	0.547 Early
*18	16.74	0.06	2.98	5.29	2.31	0.6	E/S0	0.000 M star
16	16.89	0.05	2.58	5.47	2.89	0.55	E/S0	—
24	16.89	0.07	2.69	5.61	2.92	0.55	E/S0	—
37	16.91	0.05	2.40	5.32	2.92	0.45–0.6	E/S0	0.537 Poor s/n
55	17.00	0.05	2.59	5.45	2.86	0.55	E/S0	—
56	17.11	0.06	1.71	4.42	2.71	0.1–0.2	Sab	0.398 Early
30	17.13	0.19	2.43	5.05	2.62	0.55	E/S0	—
61	17.16	0.08	2.39	5.26	2.87	0.45–0.55	E/S0	—
22	17.19	0.09	2.38	5.54	3.16	0.45–0.55	E/S0	—
129	17.21	0.14	2.52	5.44	2.92	0.6	E/S0	—
59	17.22	0.06	1.95	4.61	2.66	0.2–0.3	Sab	0.209
151	17.23	0.13	—	5.87	—	—	—	—
126	17.23	0.10	2.16	5.43	3.27	0.3	E/S0	—
31	17.25	0.18	2.39	5.98	3.59	—	—	—
145	17.25	0.09	2.51	5.50	2.99	—	—	—
57	17.28	0.07	2.65	5.41	2.76	0.55	Sab	—

Table 4 (a) – *continued*

#	K	σ_K^*	$(V-I)^*$	$(V-K)^*$	$(I-K)^*$	$\sim z^\dagger$	Class†	Spectroscopy‡
17	17.28	0.06	2.57	5.42	2.85	0.3/0.6	Sab/Scd	—
124	17.38	0.13	2.37	5.57	3.20	—	—	—
21	17.43	0.11	2.12	5.14	3.02	0.5–0.55	Sbc	—
47	17.45	0.08	2.58	5.56	2.98	—	—	—
150	17.48	0.15	1.53	4.09	2.56	0.2–0.3	Scd	—
13	17.51	0.08	2.50	5.72	3.22	—	—	—
64	17.53	0.24	1.94	4.60	2.66	0.3	E/S0	0.556 PSG
33	17.57	0.11	2.49	5.65	3.16	—	—	—
46	17.61	0.11	2.54	5.47	2.93	—	—	0.548 Early
128	17.62	0.14	2.31	5.22	2.91	—	—	—
D406	17.64	0.15	2.30	5.23	2.93	—	—	—
4	17.69	0.15	1.63	4.62	2.99	>0.45	Sdm	0.658 [OII]
60	17.71	0.09	2.59	5.42	2.83	—	—	—
132	17.75	0.15	2.53	6.88	4.35	—	—	—
36	17.75	0.10	1.60	5.33	3.73	—	—	—
127	17.79	0.12	2.43	5.29	2.86	—	—	—
5	17.80	0.14	2.17	5.25	3.08	—	—	—
51	17.81	0.12	2.43	5.32	2.89	—	—	—
65	17.87	0.26	2.38	6.37	3.99	—	—	—
D405	17.99	0.14	1.83	4.84	3.01	—	—	—
23	18.01	0.19	2.47	5.45	2.98	—	—	—
*76	18.01	0.15	3.05	5.29	2.24	—	—	—
75	18.02	0.19	2.29	5.30	3.01	—	—	—
130	18.09	0.17	1.89	4.47	2.58	0.3	E/S0	—

Notes: *the errors in V and I are negligible when compared with σ_K; †from Ellis et al. (1985) – SED 'redshift'; ‡from Dressler & Gunn (1992) – spectroscopic redshift; E/S0 – normal elliptical; Sab, Sbc, Scd, Sdm – spirals; PSG – post-starburst galaxy (i.e. early-type SED with strong Balmer lines).

Table 4. (b) J1888.16CL: aperture = 4.8 arcsec; $K \lesssim 18.4$ mag.

#	K	σ_K	$(V-I)$	σ_{V-I}	$(V-K)$	σ_{V-K}	$(I-K)$	σ_{I-K}
1	15.86	0.03	2.22	0.02	5.39	0.04	3.17	0.03
31	15.94	0.03	1.09	0.01	3.66	0.03	2.57	0.03
5	16.28	0.05	2.13	0.04	5.36	0.06	3.23	0.05
27	16.67	0.05	2.15	0.04	5.21	0.06	3.06	0.05
21	17.10	0.10	2.31	0.07	5.61	0.12	3.30	0.10
26	17.19	0.08	1.83	0.05	4.93	0.09	3.10	0.09
22	17.26	0.12	2.02	0.06	5.20	0.13	3.18	0.12
46	17.26	0.12	1.66	0.04	4.56	0.12	2.90	0.12
15	17.37	0.11	2.18	0.08	5.49	0.13	3.31	0.12
28	17.55	0.18	2.14	0.06	4.89	0.19	2.75	0.18
2	17.73	0.13	1.86	0.06	4.79	0.14	2.93	0.14
A3	17.79	0.20	1.00	0.13	5.41	0.23	4.41	0.21
A1	17.83	0.18	1.44	0.18	4.91	0.23	3.47	0.21
30	17.87	0.23	1.73	0.06	4.68	0.24	2.95	0.23
7	17.87	0.16	1.82	0.04	3.95	0.16	2.13	0.16
14	18.05	0.20	1.42	0.06	4.18	0.20	2.76	0.20
A2	18.08	0.23	0.73	0.29	5.44	0.27	4.71	0.34
11	18.19	0.22	1.76	0.14	5.13	0.25	3.37	0.23

4 COLOUR EVOLUTION

4.1 Colour–magnitude and colour–colour diagrams

The colour–magnitude (C–M) diagram for a given cluster enables us to identify the *red* members that we can expect to be the high-redshift counterparts of nearby cluster E/S0s (MacLaren et al. 1988; AES; Bower et al. 1992b, hereafter BLE). As our galaxies are selected in K, we use K luminosities in all the C–M diagrams. The basis of our evolutionary test for these red members is to track changes in the mean location of this locus or 'red envelope' (O'Connell 1988) with redshift. In making comparisons with present-day ellipticals, we adhere to the policy of displaying *raw* data for the high-redshift samples.

4.1.1 *Non-evolutionary predictions*

To predict the baseline 'no evolution' position of the C–M diagram at a given redshift, we use BLE's data for the Coma

Table 4. (c) Cl0317+1521: aperture = 4.8 arcsec; $K \lesssim 18.3$ mag.

#	K	σ_K	$(V-I)$	σ_{V-I}	$(V-K)$	σ_{V-K}	$(I-K)$	σ_{I-K}
*12	16.40	0.05	3.11	0.07	5.54	0.08	2.43	0.05
*16	16.60	0.06	1.60	0.01	3.36	0.06	1.76	0.06
4	16.65	0.06	1.83	0.06	4.93	0.08	3.10	0.07
3	16.88	0.08	2.08	0.07	4.97	0.10	2.89	0.08
*10	17.10	0.11	2.17	0.04	4.31	0.12	2.14	0.11
1	17.11	0.11	1.88	0.09	5.02	0.14	3.14	0.12
5	17.13	0.08	1.67	0.10	4.99	0.12	3.32	0.10
14	17.59	0.14	1.95	0.10	4.67	0.17	2.72	0.14
*8	17.62	0.18	2.64	0.14	5.03	0.22	2.40	0.18
*18	17.67	0.15	3.00	0.37	5.67	0.40	2.67	0.15
6	17.99	0.19	1.29	0.09	3.79	0.20	2.50	0.20
9	18.12	0.20	1.24	0.06	3.33	0.20	2.09	0.20
15	18.12	0.20	1.22	0.14	4.13	0.23	2.91	0.22

Table 4. (d) F1767.10TC: aperture = 6.4 arcsec; $K \lesssim 18.0$ mag.

#	K	σ_K	$(V-I)$	σ_{VI}	$(V-K)$	σ_{VK}	$(I-K)$	σ_{IK}	$\sim z^{\dagger}$	Class†	$z^{\dagger}_{spec}$
44(d)	16.15	0.05	2.57	0.09	5.75	0.10	3.18	0.06	0.66	E/S0	0.663
65(g)	16.31	0.05	2.20	0.07	5.00	0.08	2.80	0.06	0.66	E/S0+uvx	0.665
39	16.47	0.06	2.75	0.14	5.66	0.15	2.91	0.07	0.72	E/S0	
54(e)	16.76	0.06	2.42	0.10	5.15	0.11	2.73	0.07	0.66	E/S0	0.673
28(c)	16.93	0.09	2.36	0.12	5.15	0.14	2.79	0.10	0.66	E/S0	0.653
52	17.17	0.10	2.51	0.08	5.36	0.12	2.85	0.12	0.4	E/S0	
63	17.21	0.10	2.75	0.21	5.57	0.22	2.82	0.12	0.66	E/S0	
40(a)	17.36	0.14	1.37	0.06	3.92	0.15	2.55	0.15	0.4–0.5	Sab	0.562
53	17.48	0.11	2.59	0.25	5.52	0.26	2.93	0.13	0.72	E/S0	
43	17.53	0.16	2.34	0.16	5.00	0.22	2.66	0.17	0.66	E/S0	
64	17.60	0.15	3.03	0.08	4.96	0.17	1.93	0.16	0.66	E/S0+uvx	
46	17.90	0.22	2.30	0.20	4.85	0.28	2.55	0.23	0.66	E/S0	
45	17.91	0.20	1.96	0.18	5.00	0.26	2.64	0.22	0.4–0.5	E/S0	
48	17.92	0.21	2.44	0.22	4.92	0.30	2.48	0.22	0.66	E/S0	
42	17.93	0.22	2.25	0.29	5.28	0.35	3.03	0.25	0.44	E/S0	
49	17.93	0.21	1.92	0.21	4.76	0.28	2.84	0.24	0.4–0.45	E/S0	

Notes: †photometric redshift and classification; ‡from Couch et al. (1991); E/S0 – normal elliptical; E/S0 + uvx – elliptical galaxy with UV excess; Sab, Sbc, Scd, Sdm – spirals.

Table 4. (e) Cl1322+3029: aperture = 6.4 arcsec; $K \lesssim 18.0$ mag.

#	K	σ_K	$(V-I)$	σ_{V-I}	$(V-K)$	σ_{V-K}	$(I-K)$	σ_{I-K}
5	16.04	0.06	2.70	0.07	5.96	0.09	3.27	0.06
1	16.05	0.05	2.65	0.07	5.73	0.08	3.08	0.05
33	16.11	0.08	1.36	0.02	3.86	0.08	2.50	0.08
3	16.68	0.08	2.93	0.20	6.26	0.21	3.33	0.09
*6	16.88	0.11	2.64	0.08	5.13	0.13	2.49	0.11
16	17.05	0.11	1.50	0.05	4.32	0.12	2.82	0.12
21	17.17	0.13	1.70	0.07	4.56	0.14	2.87	0.14
7	17.23	0.13	1.78	0.15	5.29	0.18	3.51	0.15
40	17.28	0.20	1.79	0.45	6.42	0.38	4.63	0.37
8	17.45	0.19	2.31	0.26	5.80	0.31	3.50	0.21
20	17.51	0.23	1.81	0.22	5.44	0.30	3.63	0.26
32	17.70	0.20	2.35	0.16	5.25	0.25	2.90	0.21
4	17.88	0.27	1.83	0.11	4.35	0.29	2.52	0.28
13	17.89	0.27	1.34	0.17	4.63	0.30	3.29	0.30

cluster for which precise photometric and morphological information exists. In doing this, of course, we are assuming that the Coma early types are representative of all such local populations – a point discussed in detail by BLE. Since the evolutionary changes in colour are likely to be small, it is important that the predictions are precise. This is not a trivial issue, because the photometric bands used at high redshift sample rest wavelengths that vary from cluster to cluster and are quite distinct from those in the Coma cluster. The standard approach, whereby colours are reduced to their zero-

Table 4. (f) Cl0020 + 0407: aperture = 4.8 arcsec; $K \lesssim 18.4$ mag.

#	K	σ_K	$(V-I)$	σ_{V-I}	$(V-K)$	σ_{V-K}	$(I-K)$	σ_{I-K}
2	16.62	0.05	2.47	0.06	5.68	0.07	3.21	0.07
17	17.10	0.06	2.21	0.07	5.16	0.07	2.95	0.08
13	17.18	0.09	2.69	0.10	5.82	0.11	3.13	0.11
1	17.38	0.09	2.50	0.12	5.58	0.13	3.08	0.12
12	17.62	0.11	1.55	0.06	4.01	0.11	2.46	0.12
11	17.63	0.11	1.90	0.07	4.53	0.12	2.63	0.13
4	17.73	0.13	2.10	0.12	5.14	0.15	3.04	0.16
19	17.81	0.13	2.84	0.14	5.72	0.17	2.87	0.15
9	17.85	0.14	1.83	0.23	5.49	0.17	3.66	0.24
10	17.96	0.15	1.19	0.05	3.25	0.15	2.06	0.16
3	18.09	0.18	2.98	0.29	6.16	0.31	3.17	0.24
6	18.13	0.18	> 2.50	—	> 6.70	—	4.27	0.46
14	18.17	0.16	2.42	0.27	5.79	0.24	3.36	0.25
8	18.22	0.18	2.34	0.16	5.15	0.20	2.81	0.22
22	18.26	0.19	1.29	0.13	4.11	0.20	2.82	0.23

Table 4. (g) Cl1322 + 3027: aperture = 4.8 arcsec; $K \lesssim 18.2$ mag.

#	K	σ_K	$(V-I)$	σ_{V-I}	$(V-K)$	σ_{V-K}	$(I-K)$	σ_{I-K}
*6	16.33	0.05	2.83	0.04	5.22	0.06	2.39	0.05
1	16.38	0.05	2.77	0.11	6.02	0.12	3.25	0.05
2	16.55	0.05	2.74	0.09	6.05	0.10	3.31	0.05
3	16.84	0.07	2.78	0.19	6.17	0.20	3.39	0.08
7	16.97	0.07	2.59	0.19	5.97	0.20	3.39	0.08
5	17.38	0.10	2.99	0.39	6.38	0.40	3.39	0.11
14	17.42	0.10	2.10	0.16	5.49	0.18	3.39	0.12
*11	17.58	0.13	0.99	0.01	2.40	0.13	1.41	0.13
4	17.60	0.12	2.78	0.31	5.90	0.33	3.12	0.13
9	17.85	0.13	1.72	0.21	4.88	0.24	3.17	0.14
12	17.91	0.18	2.58	0.30	5.73	0.35	3.15	0.19
10	17.91	0.16	2.28	0.23	5.35	0.27	3.07	0.17
8	17.96	0.16	1.25	0.23	5.06	0.25	3.81	0.21

Table 4. (h) Cl2155 + 0334: aperture = 6.4 arcsec; $K \lesssim 19.3$ mag.

#	K	σ_K	$(V-I)$	σ_{V-I}	$(V-K)$	σ_{V-K}	$(I-K)$	σ_{I-K}
1	16.49	0.04	2.49	0.02	4.74	0.04	2.25	0.04
*14	16.97	0.05	2.45	0.02	4.07	0.05	1.62	0.05
19	17.29	0.06	2.52	0.07	5.28	0.08	2.76	0.07
12	17.60	0.07	2.20	0.09	4.87	0.10	2.67	0.09
18	17.95	0.09	1.85	0.15	5.12	0.13	3.27	0.15
*4	18.19	0.10	3.10	0.09	4.90	0.13	1.80	0.11
15	18.24	0.10	1.99	0.18	5.09	0.17	3.10	0.15
5	18.29	0.11	3.05	0.18	5.43	0.19	2.38	0.14
3	18.62	0.15	2.54	0.16	4.81	0.19	2.27	0.18
20	18.71	0.17	1.43	0.36	4.97	0.23	3.54	0.36
7	19.00	0.16	2.04	0.11	3.85	0.18	1.81	0.18
8	19.08	0.18	1.95	0.11	3.72	0.20	1.77	0.20
10	19.11	0.20	1.61	0.18	4.06	0.23	2.45	0.24
6	19.14	0.20	2.23	0.20	4.44	0.25	2.21	0.24
13	19.17	0.25	1.50	0.14	3.47	0.26	1.97	0.28

redshift equivalent using *k-corrections* calculated from local SEDs, is insufficiently precise for our purposes. Instead, we choose to link the observed *VIK* photometric bands used in the distant clusters with the photometric bands that lie closest to their rest-frame equivalents for a given cluster. Here we use BLE's photometry of E/S0 galaxies in Coma to construct the appropriate *no-evolution* C–M diagram at high z. This procedure, also used by AES, has the advantages that it is based on empirical data which include the slope of the C–M relation and that, to first order, it eliminates the need to calculate k-corrections. In practice, of course, no photometric passbands for which Coma data are available perfectly match the rest-frame versions of those used at high redshift, and second-order corrections have to be made to allow for this. The procedure adopted is as described by AES, and we briefly review it here.

The observed K band corresponds to a rest-frame $\lambda_{\rm eff}$ between the J and H bands for $0.55 < z < 0.76$ and slightly

Table 4. (i) Cl1603+4313: aperture = 4.8 arcsec; $K \lesssim 19.5$ mag.

#	K	σ_K	$(V-I)$	σ_{V-I}	$(V-K)$	σ_{V-K}	$(I-K)$	σ_{I-K}
7	17.00	0.05	2.74	0.06	6.36	0.08	3.62	0.05
5	17.01	0.05	2.87	0.06	6.45	0.08	3.58	0.05
1	17.07	0.05	2.44	0.04	5.91	0.06	3.47	0.05
2	17.63	0.06	2.56	0.08	6.13	0.10	3.57	0.06
17	18.02	0.12	2.88	0.08	5.74	0.14	2.86	0.12
*18	18.06	0.14	2.63	0.03	4.52	0.14	1.89	0.14
11	18.07	0.10	2.07	0.09	5.75	0.13	3.68	0.10
23	18.22	0.09	2.03	0.06	5.26	0.11	3.23	0.09
6	18.26	0.10	1.44	0.08	5.35	0.12	3.91	0.11
3	18.40	0.10	1.84	0.14	5.80	0.16	3.96	0.11
10	18.48	0.11	2.41	0.16	5.95	0.19	3.54	0.12
8	18.54	0.15	> 1.40	—	> 6.70	—	5.46	0.27
24	18.85	0.14	1.73	0.12	5.24	0.18	3.51	0.15
4	18.96	0.14	0.53	0.05	3.68	0.14	3.15	0.15
20	19.05	0.20	> 1.50	—	> 6.20	—	4.79	0.27
16	19.07	0.27	1.66	0.10	4.74	0.28	3.08	0.27
22	19.19	0.20	2.51	0.22	5.62	0.30	3.11	0.20
12	19.20	0.16	2.84	0.44	6.34	0.46	3.50	0.17
*13	19.29	0.28	2.22	0.07	4.31	0.29	2.09	0.28

Table 4. (j) Cl1603+4329: aperture = 4.8 arcsec; $K \lesssim 19.0$ mag.

#	K	σ_K	$(V-I)$	σ_{V-I}	$(V-K)$	σ_{V-K}	$(I-K)$	σ_{I-K}
8	17.59	0.08	2.07	0.23	6.21	0.22	4.14	0.14
1	17.62	0.09	1.96	0.17	5.74	0.17	3.78	0.12
14	17.73	0.11	1.69	0.12	5.09	0.15	3.40	0.13
19	17.74	0.09	2.44	0.19	5.77	0.20	3.33	0.11
2	17.75	0.11	2.79	0.28	6.24	0.29	3.45	0.13
*21	17.76	0.10	3.63	0.55	7.20	0.56	3.57	0.12
15	17.83	0.11	1.42	0.09	4.49	0.13	3.07	0.13
4	17.93	0.11	2.14	0.20	5.62	0.21	3.48	0.14
18	18.14	0.16	1.99	0.25	5.68	0.27	3.69	0.20
10	18.19	0.13	2.79	0.52	6.32	0.52	3.53	0.18
5	18.40	0.17	> 2.42	—	> 6.55	—	4.13	0.29
11	18.45	0.15	1.38	0.35	5.49	0.30	4.11	0.27
7	18.49	0.17	1.82	0.18	4.71	0.23	2.89	0.19
6	18.58	0.18	1.54	0.13	4.30	0.21	2.76	0.20
3	18.59	0.17	2.17	0.20	5.02	0.25	2.85	0.19
20	18.65	0.21	1.63	0.16	4.66	0.25	3.03	0.23
22	18.73	0.20	2.75	0.37	5.77	0.41	3.02	0.22
*23	18.83	0.20	> 3.30	—	> 6.10	—	2.78	0.25
25	18.83	0.20	3.12	0.60	6.03	0.62	2.91	0.23
17	18.92	0.21	1.20	0.10	3.49	0.22	2.29	0.22

shortward of J for $0.76 < z < 0.9$. A linear transformation between observed $K(z)$ at a given z and rest-frame J_0 is calculated as a function of the rest-frame $(J-H)_0$ colour using the appropriate filter response curves (UKIRT Observer's Manual 1989, 1991) and infrared SEDs for types E/S0–Sdm (as described in AES, with the addition of those presented in Yoshii & Takahara 1988). The rms scatter on the K transformations as determined for the range of SEDs (see AES) is smaller than 0.02 mag for all clusters, and is typically only 0.014 mag.

In a similar manner, the I band corresponds to rest-frame effective wavelengths near or blueward of the V band for our clusters, and a linear transformation between $I(z)$ and V_0 as a function of $(U-V)_0$ can be computed as before, with an average rms of 0.02 mag for the complete range of SEDs. Finally, the V band corresponds approximately to U_0, and a transformation between $V(z)$ and U_0 as a function of $(U-V)_0$ can be constructed. The $(U-V)_0$ dependence here is relatively weak for the E/S0 SEDs (which cover a very broad range of UV spectral shapes and colours), and suitable functions (from a constant to a second-order polynomial) are fitted in each case. The scatter around the adopted transformations is 0.02 mag, increasing slightly for the two highest z clusters.

Table 5 summarizes the transformations between the observed *VIK* and the rest-frame *UVJH* magnitudes for each cluster, together with an estimate of the internal uncertainty. In each case, the photometric response curves correspond to the precise filter + detector combinations used, which vary slightly according to the instrumentation. These equations are used to transform BLE's Coma galaxy photometry, having first corrected for aperture effects with the V growth curve of Sandage & Visvanathan (1978) and mean colour gradients of $\Delta(V-K)/\Delta \log[A/D(0)] = -0.1$ and

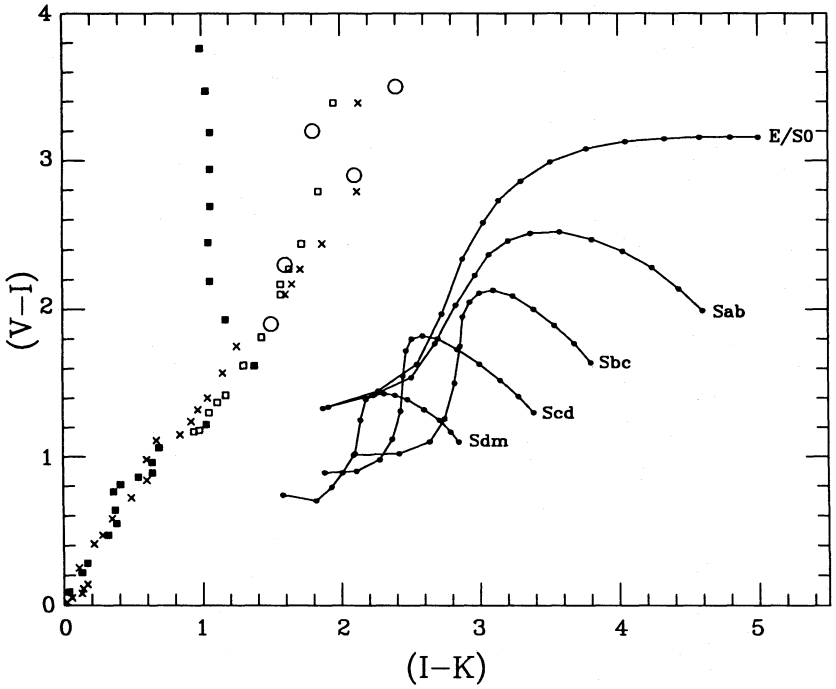

Figure 4. Expected position of the Galactic stars on the $(V-I)$ versus $(I-K)$ plane. Filled squares are main-sequence stars, open squares are giants and crosses are supergiants (Johnson 1966; Koornneef 1983). Large open circles represent the stars that Cowie et al. (1992) found in their deep field images. For comparison, filled circles connected with solid lines show the loci of different types of galaxy as a function of redshift (with no evolution). The bluest point of each track in $(I-K)$ corresponds to $z=0$ and the reddest to $z=1.4$ in steps of 0.1.

$\Delta(U-V)/\Delta \log[A/D(0)] = -0.15$ (Sandage & Visvanathan 1978; Persson, Frogel & Aaronson 1979; Peletier et al. 1990). The local data are converted to an aperture equivalent to the observed 4.8- or 6.4-arcsec diameter, corresponding to projected linear sizes of 38 and 51 kpc respectively at the average redshift of the cluster sample, $\langle z\rangle = 0.71$ (we adopt $H_0 = 50$ km s^{-1} Mpc^{-1}, $q_0 = 0.5$ throughout). The transformed magnitudes and colours define a no-evolution C–M locus for each cluster (see Table 5).

Although the internal errors are small and well understood, systematic errors on our no-evolution prediction may arise. However, whereas inappropriate SEDs would introduce sizeable systematic errors when computing predictions based on the *k*-corrections, because we predict an observed magnitude M_z not from a rest-frame M_0 but from a rest-frame M_0' whose effective wavelength lies close to that of M_z, the transformation is much less dependent on the SED. As a test of possible systematic uncertainties, we have computed similar transformations based on Persson et al.'s (1979) E/S0 photometry in *UBVRJHK*. These agree well with those based on BLE, and on this basis we estimated systematic uncertainties to be $\lesssim 0.05$ mag (see Aragón-Salamanca 1991 for details).

Although Galactic reddening could significantly affect the observed colours, the Galactic latitudes are high enough in most cases to make the likely effect small. As detailed reddening estimates in the relevant directions are not available, we have used the Burstein & Heiles (1982) H I maps to estimate $E(B-V)$. These authors claimed that their *relative* reddening scale should be accurate to within 0.01 in $E(B-V)$ or 10 per cent in A_λ (whichever is largest). Since we are comparing relative changes in colour for the different clusters, this should not introduce significant uncertainties, particularly as we apply a similar reddening correction for the Coma data.

Using these $E(B-V)$ values and the Galactic extinction law (Savage & Mathis 1979; Mathis 1990), we have computed the extinction in each band. The estimated relative uncertainty in $E(B-V)$ translates into relative (cluster to cluster) uncertainties in the absorption corrections of the order of $\delta A_V \sim 0.03$ mag, $\delta A_I \sim 0.02$ mag and $\delta A_K \sim 0.004$ mag. The adopted $E(B-V)$ colour excesses are presented in the last column of Table 5.

4.1.2 *Colour–magnitude diagrams*

The small number of objects per cluster and the lack of membership information prevent us from drawing any strong conclusion from C–M diagrams for individual clusters. To improve the statistics, we have combined the different clusters in three convenient redshift bins: 0016+16, J1888.16CL and Cl0317+1521 ($\langle z\rangle = 0.56$); F1767.10TC, Cl1322+3029, Cl0020+0407 and Cl1322+3027 ($\langle z\rangle = 0.70$); and Cl2155+0334, Cl1603+4313 and Cl1603+4329 ($\langle z\rangle = 0.88$). In combining three or four clusters in this way, we make additional small corrections for the differential effects of redshift across the narrow range, as well as for small differences in the photometric systems. At first sight, this would seem dangerous since, ideally, redshifts and SEDs are required for all the objects sampled. However, since the redshift bins are relatively narrow, it can be done

with sufficient precision for our purposes in the following way.

Colours are zero-pointed to the reddening-corrected no-evolution C–M locus by subtracting the predicted colour (at the observed K magnitude) from the observed colour. We refer to the relative colours as $\Delta(V-I)$, $\Delta(V-K)$ and $\Delta(I-K)$, such that $\Delta(\text{colour})=0.0$ refers to a non-evolving present-day elliptical at the chosen mean redshift. For the field objects and the non-elliptical members, this is only strictly correct to first order, since these objects presumably have different SEDs. However, the redshift increment is so small ($\Delta z<0.05$) that the residual correction is negligible and will not, therefore, introduce any significant additional uncertainty. To make this point clear, the difference between the relative corrections for an E/S0 and an Sdm across a typical redshift bin is <0.02 in $(V-I)$ or <0.03 in $(I-K)$. Magnitudes are corrected for relative distance modulus differences and the differential k-corrections introduce

Table 5. No-evolution predictions.

Cluster	z	Photometric transformations	*r.m.s.*	C-M relations	$E(B-V)$
0016+16	0.546	$U_o - V_z = -0.42$	0.020	$(V-I) = 4.520 - 0.096 \times I$	0.03
		$V_o - I_z = 0.78$	0.020	$(V-K) = 8.620 - 0.173 \times K$	
		$J_o - K_z = 1.265 + 0.491 \times (J-H)_o$	0.020	$(I-K) = 4.520 - 0.084 \times K$	
J1888.16CL	0.563	$U_o - V_z = -0.45$	0.020	$(V-I) = 4.460 - 0.090 \times I$	0.00
		$V_o - I_z = 0.898 - 0.063 \times (U-V)_o$	0.012	$(V-K) = 8.639 - 0.172 \times K$	
		$J_o - K_z = 1.301 + 0.445 \times (J-H)_o$	0.020	$(I-K) = 4.678 - 0.094 \times K$	
Cl0317+1521	0.583	$U_o - V_z = -0.51$	0.015	$(V-I) = 4.392 - 0.086 \times I$	0.12
		$V_o - I_z = 0.892 - 0.102 \times (U-V)_o$	0.020	$(V-K) = 8.679 - 0.169 \times K$	
		$J_o - K_z = 1.383 + 0.332 \times (J-H)_o$	0.015	$(I-K) = 4.631 - 0.088 \times K$	
F1767.10TC	0.664	$U_o - V_z = -0.711$	0.020	$(V-I) = 4.339 - 0.077 \times I$	0.00
		$V_o - I_z = 0.893 - 0.153 \times (U-V)_o$	0.017	$(V-K) = 8.722 - 0.160 \times K$	
		$J_o - K_z = 1.475 + 0.219 \times (J-H)_o$	0.019	$(I-K) = 4.689 - 0.087 \times K$	
Cl1322+3029	0.697	$U_o - V_z = -0.985 + 0.384 \times (U-V)_o - 0.170 \times (U-V)_o^2$	0.014	$(V-I) = 4.365 - 0.078 \times I$	0.00
		$V_o - I_z = 0.883 - 0.213 \times (U-V)_o$	0.023	$(V-K) = 8.976 - 0.166 \times K$	
		$J_o - K_z = 1.555 + 0.110 \times (J-H)_o$	0.012	$(I-K) = 4.945 - 0.092 \times K$	
Cl0020+0407	0.698	$U_o - V_z = -1.012 + 0.407 \times (U-V)_o - 0.175 \times (U-V)_o^2$	0.017	$(V-I) = 4.484 - 0.082 \times I$	0.03
		$V_o - I_z = 0.896 - 0.213 \times (U-V)_o$	0.020	$(V-K) = 9.122 - 0.174 \times K$	
		$J_o - K_z = 1.555 + 0.110 \times (J-H)_o$	0.013	$(I-K) = 4.991 - 0.097 \times K$	
Cl1322+3027	0.751	$U_o - V_z = -0.92$	0.017	$(V-I) = 4.284 - 0.070 \times I$	0.00
		$V_o - I_z = 0.868 - 0.266 \times (U-V)_o$	0.025	$(V-K) = 9.191 - 0.168 \times K$	
		$J_o - K_z = 1.620 + 0.027 \times (J-H)_o$	0.007	$(I-K) = 5.216 - 0.102 \times K$	
Cl2155+0334	0.820	$U_o - V_z = -1.285 + 0.363 \times (U-V)_o - 0.227 \times (U-V)_o^2$	0.017	$(V-I) = 4.867 - 0.087 \times I$	0.06
		$V_o - I_z = 0.865 - 0.340 \times (U-V)_o$	0.019	$(V-K) = 10.040 - 0.197 \times K$	
		$J_o - K_z = 1.696 - 0.073 \times (J-H)_o$	0.003	$(I-K) = 5.507 - 0.111 \times K$	
Cl1603+4313	0.895	$U_o - V_z = -1.233 - 0.015 \times (U-V)_o - 0.125 \times (U-V)_o^2$	0.041	$(V-I) = 4.826 - 0.083 \times I$	0.00
		$V_o - I_z = 0.821 - 0.492 \times (U-V)_o$	0.022	$(V-K) = 10.496 - 0.204 \times K$	
		$J_o - K_z = 1.756 - 0.148 \times (J-H)_o$	0.014	$(I-K) = 6.079 - 0.127 \times K$	
Cl1603+4329	0.920	$U_o - V_z = -1.074 - 0.386 \times (U-V)_o$	0.047	$(V-I) = 4.846 - 0.081 \times I$	0.00
		$V_o - I_z = 0.805 - 0.535 \times (U-V)_o$	0.023	$(V-K) = 10.677 - 0.207 \times K$	
		$J_o - K_z = 1.767 - 0.162 \times (J-H)_o$	0.018	$(I-K) = 6.244 - 0.131 \times K$	

changes of $\lesssim 0.15$, regardless of the SED, and can be ignored since the C–M relations are very flat. The corrections due to the relative change in projected linear size of the photometric aperture can be neglected in both magnitude ($\lesssim 0.007$ mag) and colour ($\lesssim 0.001$ mag).

Figs 5–7 show the combined $(V-K)$ and $(I-K)$ C–M diagrams for the three redshift bins. Different symbols are used for each cluster contributing to the figure. Although these figures are clearly polluted by field objects, some obvious trends are apparent.

First, the $(I-K)$ C–M diagrams are tighter than the $(V-K)$ equivalents for all redshifts. Secondly, a clear blueing trend with redshift is seen: at $\langle z\rangle = 0.56$ there are more objects lying below the $\Delta(I-K)=0$ line than above, and the fraction of such blue objects appears to increase with z. Although this blueing trend may indicate evolution in the red envelope or blue fraction, as no attempt has yet been made to eliminate field contamination it could equally well arise from an increase with redshift in the proportion of non-members within the photometric catalogues.

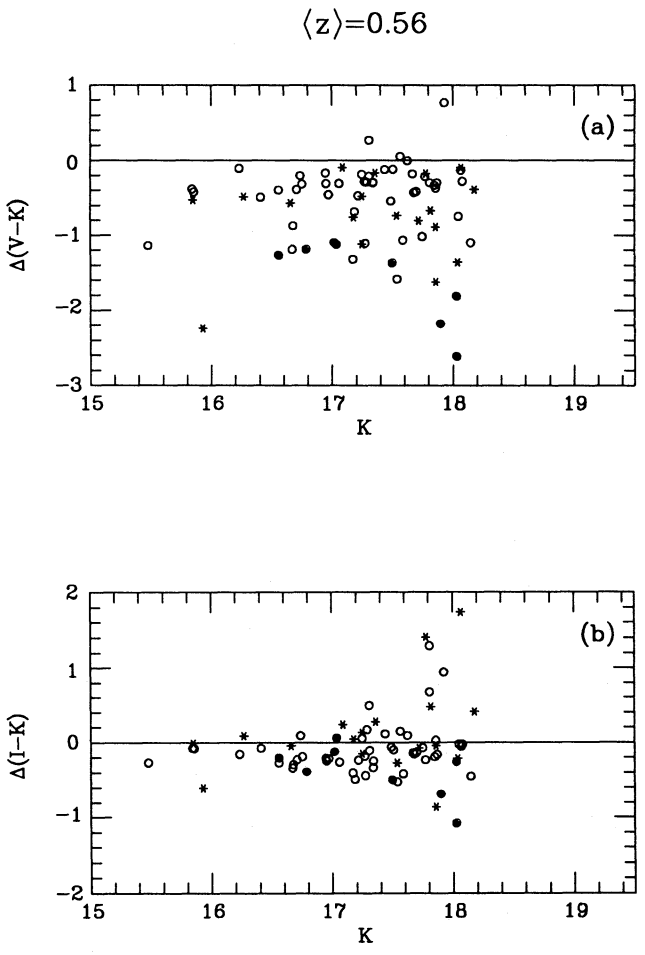

Figure 5. Combined colour–magnitude diagrams for the clusters 0016+16 (open circles), J1888.16CL (asterisks) and Cl0317+1521 (filled circles). The average redshift is $\langle z\rangle = 0.56$. See text for details.

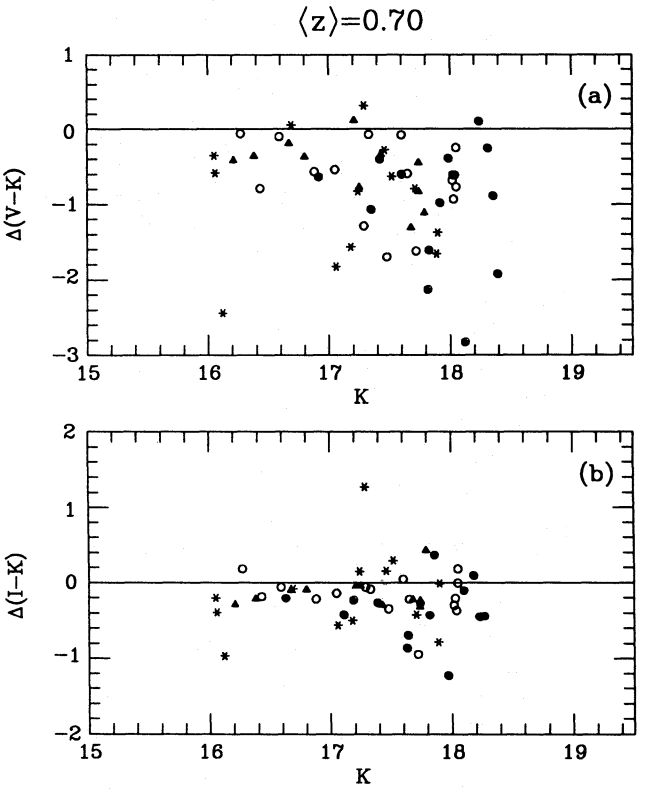

Figure 6. As Fig. 5, for F1767.10TC (open circles), Cl1322+3029 (asterisks), Cl0020+0407 (filled circles) and Cl1322+3027 (filled triangles). The average redshift is $\langle z\rangle = 0.70$.

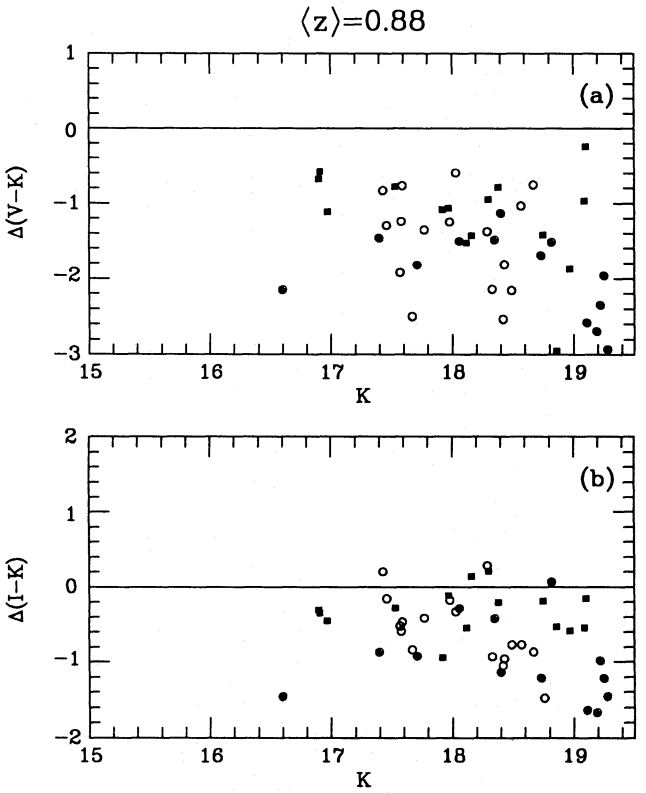

Figure 7. As Fig. 5, for Cl2155+0334 (filled circles), Cl1603+4313 (filled squares) and Cl1603+4329 (open circles). The average redshift is $\langle z\rangle = 0.88$.

4.1.3 *Colour–colour diagrams*

The $(V-I)$ versus $(I-K)$ colour–colour (C–C) diagrams show the data in a somewhat different form (Fig. 8). Here, we show the expected locus of non-evolving present-day galaxies of different spectral types as a function of redshift in the same 'system' as before (i.e. colours relative to those of an elliptical galaxy at the appropriate redshift). As expected, most objects are bluer than present-day ellipticals at these redshifts. The cluster members for $\langle z\rangle = 0.56$ and 0.70 are presumably the 'clump' of red objects near (0, 0). Both the $\langle z\rangle = 0.56$ and $\langle z\rangle = 0.70$ samples contain a few objects redder than the $\Delta(V-I) = 0.0$ line, but they are virtually absent in the $\langle z\rangle = 0.88$ diagram.

A noticeable number of objects are much redder in $(I-K)$ than the no-evolution prediction at each redshift. In principle, these sources with $\Delta(I-K) \geq 0.5$ could be background galaxies at very high z. This seems unlikely given their abundance and the implied luminosities, but if this is the case then we might expect them to share the colour evolution seen in the clusters, but for larger look-back times. We return to a discussion of these objects in Section 4.2.7.

4.2 Colour distributions

We now present the colour distributions of the field-subtracted populations, as collated from cluster data in the three redshift intervals introduced earlier. As before, all colours are normalized according to a non-evolving present-day elliptical of the appropriate luminosity.

4.2.1 *Field-corrected colour distributions*

Since membership information is not available for most of the galaxies in our sample, we have corrected for field contamination statistically. The importance of this correction will depend on the limiting K magnitude and the richness, redshift and concentration of the specific cluster. Before describing how this correction was implemented, we estimate the importance of the effect.

Following CEMM, we estimate the contrast of a cluster against the background field as a function of the cluster properties, redshift and limiting magnitude, based on the luminosity function of Abell 1942, a richness class 3 cluster at $z = 0.22$ (Couch & Newell 1984). To do this in the K passband, we adopted an appropriate mean $R-K$ colour at this redshift and used Cowie et al.'s (1992) field counts. Assuming no evolution, at $z = 0.56$ we would expect this richness to yield $N_{\rm clust} \simeq 16$ members per IRCAM frame to $K_{\rm lim} = 18.0$ mag, but only $N_{\rm field} \simeq 3$ field galaxies. The calculations can be used to estimate the optimum K limit for a given redshift, which becomes quite important at high redshifts. At $z = 0.70$, $N_{\rm clust} \simeq 16$ and $N_{\rm field} \simeq 5$ to $K_{\rm lim} = 18.5$ mag; and, for $z = 0.88$, $N_{\rm clust} \simeq 20$ and $N_{\rm field} \simeq 9$ to $K_{\rm lim} = 19.5$ mag. Although these numbers are estimates, and assume a fixed richness, they can be viewed as the best examples and thus indicate the importance of field contamination at these redshifts.

Reliance on Cowie et al.'s (1992) field counts raises two problems. First, large-scale structures could introduce greater-than-Poissonian fluctuations in the number of objects from field to field. Even if the published counts are representative, the appropriate numbers for our cluster fields may be different. In fact, the observed variations in Cowie et al.'s fields are consistent with Poissonian fluctuations, and an external check based on 11 deep fields to $K \simeq 20.5$ (Aragón-Salamanca et al. 1993) confirms this behaviour and Cowie et al.'s absolute normalization. Additionally, since we combine the photometric data from 3–4 cluster areas per redshift bin, to some extent we smooth out the field-to-field fluctuations. Secondly, the *colour distribution* could, in principle, change from field to field due to localized variations in the galaxy population. This is difficult to test, since the total number of objects is small. In Cowie et al.'s sample, there are only seven objects with $K < 18.2$ mag and 20 with $K < 19.5$ mag. Fortunately, we can expect the field contamination for the bright limiting magnitudes to be small compared to the number of cluster members ($N_{\rm field} \lesssim 4$), and the accuracy of the correction is less important. For the clusters with fainter limiting magnitudes, for which the field correction becomes more critical, the statistics are much better. Although we could reduce these statistical uncertainties by *modelling* the field distributions, this would demand an understanding of the field population, negating the advantages of our empirical approach.

In the relevant magnitude range, the counts are well represented by $N(m) = 0.0126 \times 10^{0.316m}$ galaxy deg^{-2} mag^{-1}. A field colour distribution with the appropriate K limit was extracted from Cowie et al.'s data, placed in the correct colour system and subtracted from the cluster colour distribution after scaling to the expected area. The results are shown in Fig. 9 for $(V-K)$ and $(I-K)$. Some small *negative* numbers arise from uncertainties in the field contamination due to statistical fluctuations. Given the small number of objects involved, the size of the errors is compatible with Poissonian variations, and the absence of large negative numbers for the bluer colours tends to support our procedure.

4.2.2 *A test: the clusters 0016+16 and F1767.10TC*

Two of our clusters – 0016+16 and F1767.10TC – have been studied in more detail, both via unusually extensive spectroscopy (CEMM; Dressler & Gunn 1992) and via intermediate-band CCD photometry (Ellis et al. 1985, and unpublished data). We can use the additional membership and spectral classification information for these two cases (Table 4) to check the statistical procedure defined in Section 4.2.1. These comparisons are presented in Figs 10 and 11.

For 0016+16, both techniques are in close agreement; field objects are only subtracted from the blue tail of the distribution, i.e. for this cluster the photometric properties of its members can be deduced statistically without redshift information. Adopting the *biweight* method described fully in Section 4.2.4 for the determination of the mean colour of the red peak, we find a difference of only $\Delta(I-K) \simeq \Delta(V-K) \simeq 0.02$ – well within the statistical uncertainties for the sample. More significantly, the spectrophotometric data allow us to investigate the sensitivity to the inclusion of a few blue spirals. Exclusion of the objects classed as spirals shifts the biweight mean by only 0.015, indicating it to be a robust way to determine the location of the red peak.

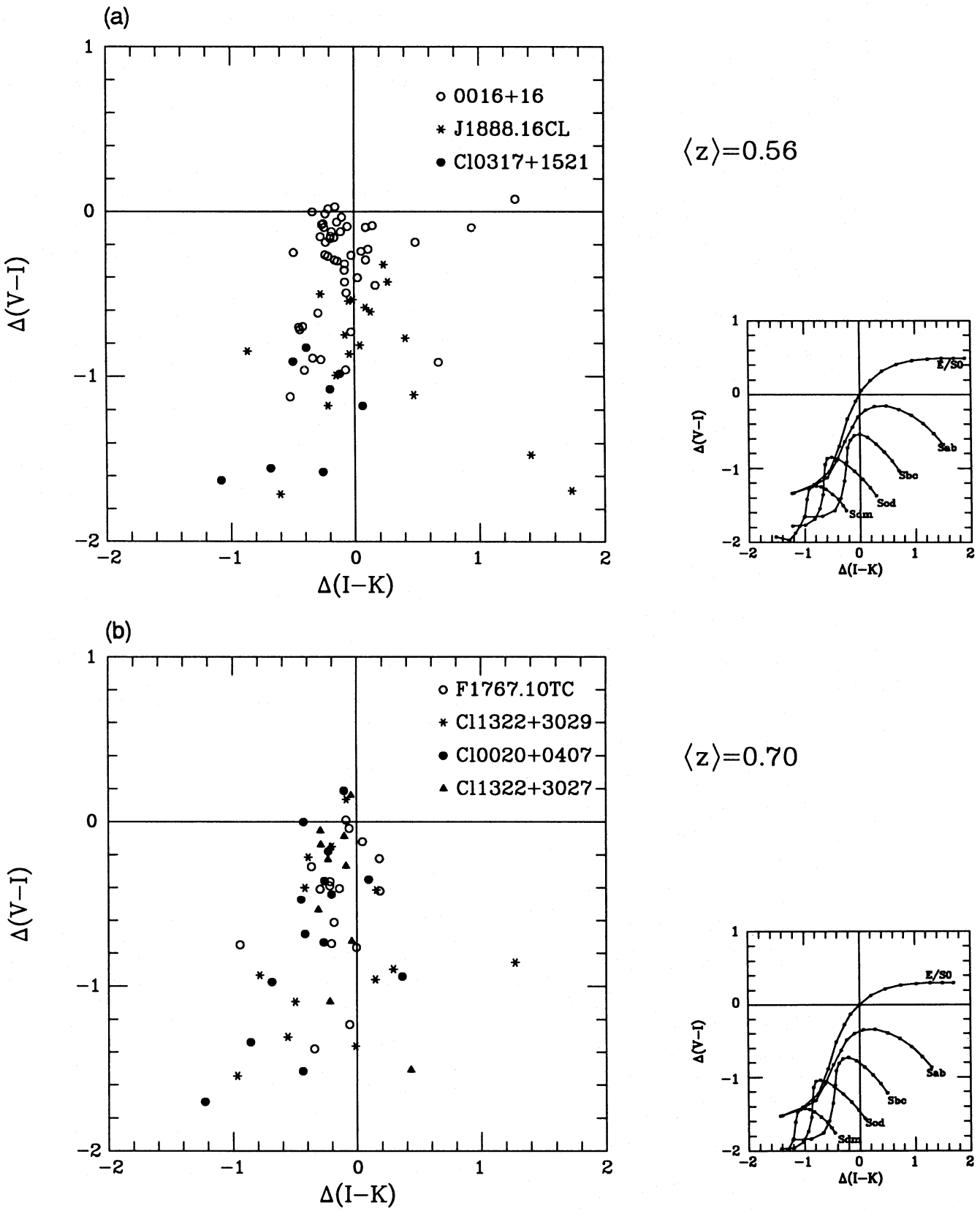

Figure 8. (a) Combined colour–colour diagram for the clusters 0016+16 (open circles), J1888.16CL (asterisks) and Cl0317+1521 (filled circles). The average redshift is $\langle z \rangle = 0.56$. See text for details. For reference, the small figure at the side shows the locus on this diagram of different types of galaxy as a function of redshift (with no evolution). The colours have been zeroed to an E/S0 at this redshift. See Fig. 4 for details. (b) As (a), for F1767.10TC (open circles), Cl1322+3029 (asterisks), Cl0020+0407 (filled circles) and Cl1322+3027 (filled triangles). The average redshift is $\langle z \rangle = 0.70$. (c) As (a), for Cl2155+0334 (filled circles), Cl1603+4313 (filled squares) and Cl1603+4329 (open circles). The average redshift is $\langle z \rangle = 0.88$.

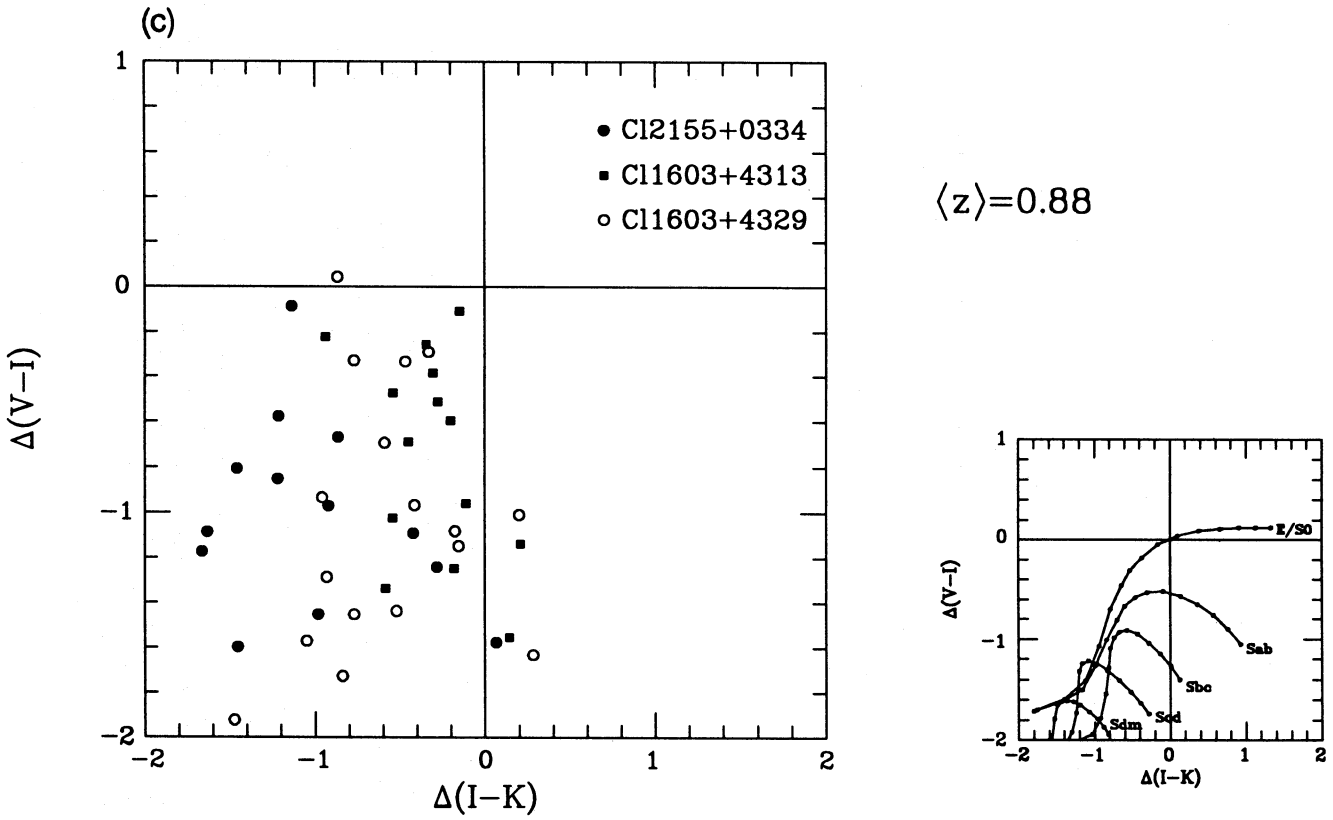

Figure 8 – *continued*

In some sense, however, this is an unfair test, given that 0016+16 is unusually rich and red. For F1767.10TC the situation is less clear (Fig. 11), for several reasons. First, the smaller number of objects increases the statistical errors. Secondly, Couch et al. (1991) found that this cluster may be partially contaminated by a foreground group at $z \sim 0.43$, which will not be accounted for in the statistical correction. Also, two of the reddest objects have photometric redshifts of 0.72 and were considered background. Since the photometric redshifts have uncertainties of 0.05 (cf. Ellis et al. 1985), these objects could be members. If we include these objects, the two methods are in reasonable agreement, considering the uncertainties.

Thus, provided that there is no severe contamination from unrelated groups along the same sight-line, our tests show that the statistical properties of the reddest cluster members can be derived from photometric data alone. Indeed, even if there is *some* contamination from *foreground* groups, the properties of the *red objects* will not appear severely distorted. Since this is the most likely problem, we point out that our goal of studying the properties of the *reddest* objects is very robust (whereas the classical Butcher–Oemler studies quantifying the *blue* tail require more precise field subtraction).

4.2.3 *Evidence for colour evolution*

We now consider the field-corrected colour distributions (Fig. 9), from which we can draw the following qualitative conclusions.

(i) In the highest redshift bin, at $\langle z \rangle = 0.88$, the *red envelope* has moved bluewards: at high redshift there are *no* galaxies with colours as red as those of present-day ellipticals. The effect is most noticeable in $(V-K)$ by virtue of the longer wavelength-baseline.

(ii) The $\Delta(I-K)$ distributions show a relatively narrow peak which moves bluewards with increasing redshift. A blue tail appears at $\langle z \rangle = 0.88$.

(iii) In $(V-K)$, the peaks are somewhat broader, but the blueing trends are stronger.

It is easy to interpret these qualitative effects in terms of simple evolutionary expectations. The shift of the red envelope at high redshift is the most significant result, since it demonstrates that *the evolutionary trend cannot solely be a continuation to higher redshift of the Butcher–Oemler effect.* Superimposed on the general ageing of the redder stellar populations is a growing blue tail, indicating that an increasing fraction of galaxies are experiencing star formation, probably linked to the Butcher–Oemler phenomenon observed at lower redshifts.

Since $(I-K)$ is sensitive to the light from the older stars born during previous major episodes of star formation, the narrow colour distribution could imply that the long-term stellar evolution from galaxy to galaxy and cluster to cluster is relatively homogeneous. While other interpretations may be consistent with the data, the simplest picture emerging is one of passive evolution from sources that formed at a common epoch.

The $(V-K)$ colour, in contrast, samples rest-frame UV

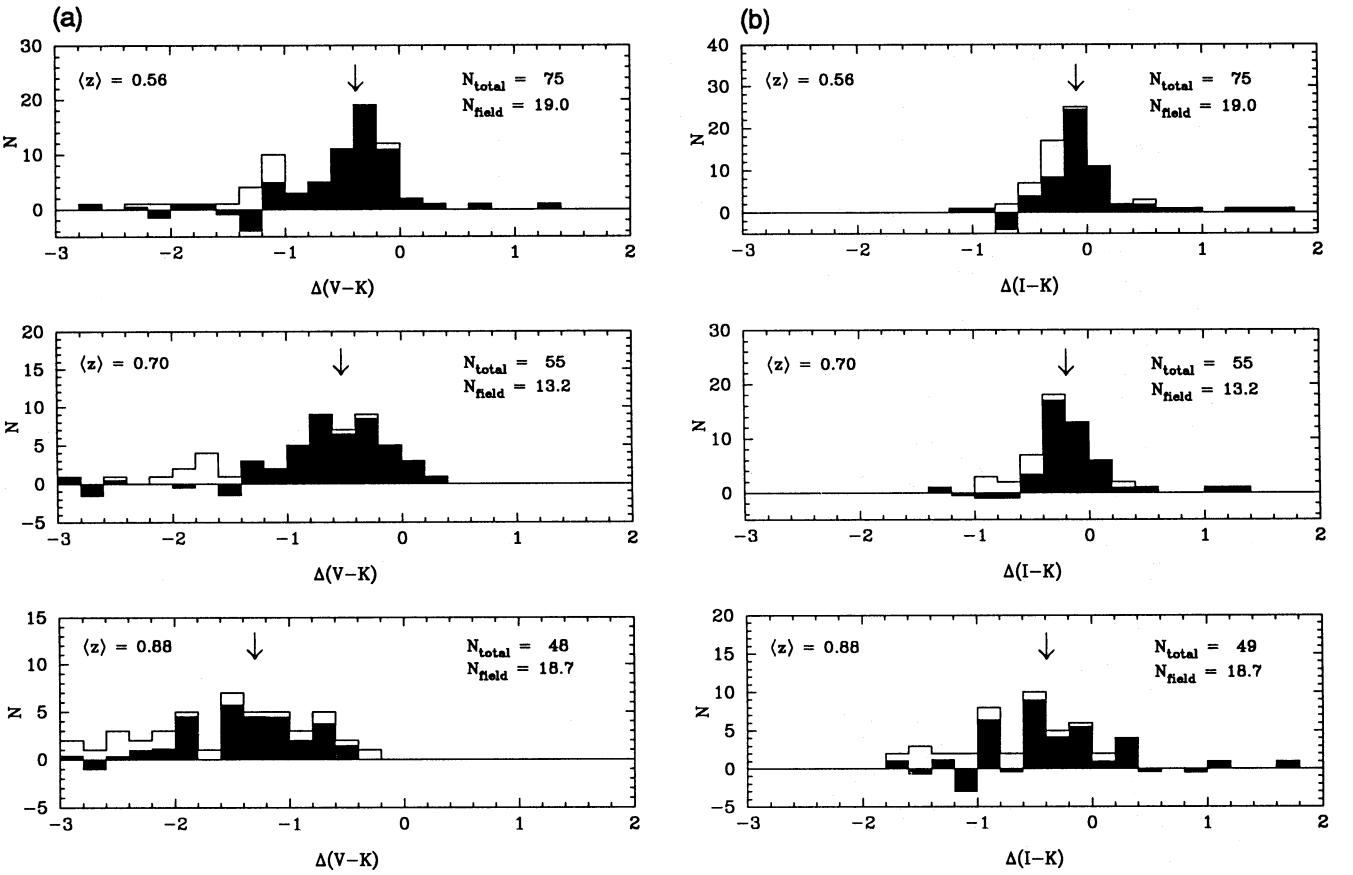

Figure 9. (a) $(V-K)$ colour distributions for the combined sample of clusters in the three redshift bins before (hollow histogram) and after (shaded) correction for field contamination. Each diagram shows the number of objects in the sample before the correction ($N_{\rm total}$) and the expected number of field objects ($N_{\rm field}$). (b) As (a), for $(I-K)$. Arrows show the colour of the red peak as determined by the biweight location estimator discussed in Section 4.2.4.

fluxes and is thus sensitive to relatively small amounts of star formation. Only a small fraction of the galaxy mass (<10 per cent) needs to be turned into stars to produce colour changes as large as those observed in the blue tails (cf. BLE). Such secondary episodes of star formation might be triggered by interaction with the intracluster medium (Dressler & Gunn 1990), or via collisions and mergers (Lavery & Henry 1988). Regardless of the mechanism, we can expect a broader distribution in $(V-K)$ compared to $(I-K)$ if secondary activities are involved. In addition, of course, a few members are likely to be normal spirals.

Despite the difficulties in disentangling the Butcher–Oemler effect, our most important result is the blueing of the red envelope, which we will now demonstrate is convincing evidence for colour evolution in representative samples of early-type galaxies, free from the biases that would distort studies of optically selected samples.

4.2.4 *Statistical analysis of the colour distributions*

In the previous section we described, qualitatively, the evolutionary trends within our sample as drawn from the field-corrected colour distributions. A more quantitative approach is needed for comparison with the predictions of evolutionary models. A major problem is that, even with field-subtracted distributions, we cannot morphologically distinguish the early-type population whose evolution we wish to track. The reddest colours presumably reflect the location of the red envelope at a given redshift, but we need to define an estimator of the mean colour that is stable to a blue tail which could be attributable to other processes or morphologies.

This problem has been discussed extensively by Beers, Flynn & Gebhardt (1990, and references therein), who gave quantitative criteria for the determination of the best estimators of the mean and standard error depending on the number of data points and the shape of the expected distribution. Following their criteria, we have adopted the *biweight* location and scale estimators ($C_{\rm BI}$ and $S_{\rm BI}$ respectively) as the most suitable for our non-Gaussian distributions, and used their *bootstrap* method to determine the confidence intervals for these estimators. We have used the code kindly provided by T. C. Beers and K. Gebhardt to perform the calculations. As this code requires all signals to be positive, we set the negative counts arbitrarily to zero prior to computing the biweight estimators. The uncertainty introduced in this procedure was estimated by adding the same *positive* signal and redoing the calculations. The changes were only $\lesssim 0.02$ mag, which we consider to be a good estimate of the reliability of the estimators. We also perturbed the expected field contamination by $\pm 1\,\sigma$ and recomputed the estimators. In all cases, $C_{\rm BI}$ and $S_{\rm BI}$ changed by less than $1\,\sigma$, demonstrating that our conclusions are insensitive to field-subtraction uncertainties. Table 6 contains the results, which will be used

in the following sections. In Fig. 9 we also mark the central location as determined from C_{BI}.

Use of the above estimator, together with the fact that we have imaged the cluster cores, should minimize the dangers of spiral contamination in the estimation of our evolutionary trends for the presumed early-type population. We can check this in the case of 0016 + 16 by using the spectral and multi-band classifications of Dressler & Gunn (1992) and Ellis et al. (1985) – see Section 4.2.2.

4.2.5 *Comparison with evolutionary models*

We now compare the amount of colour evolution detected with evolutionary models. The primary aim is to see if the changes observed are compatible with the simplest picture, whereby early-type galaxies sampled in a variety of clusters at different look-back times share a common star formation history, namely *passive* evolution following a single initial burst. A secondary goal is to parametrize this history in

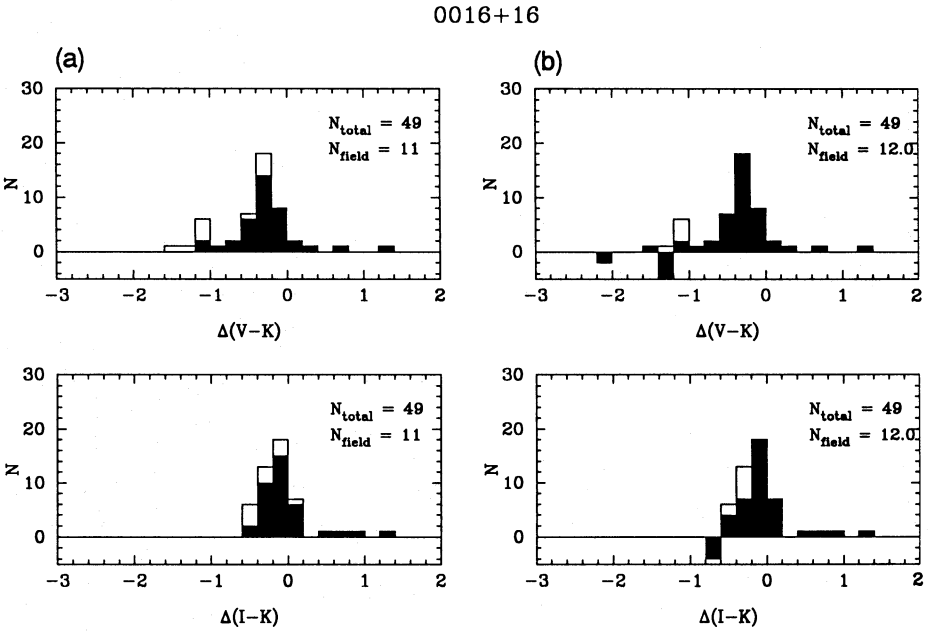

Figure 10. Test of the field contamination correction for 0016 + 16. (a) Colour distributions for all the galaxies in the sample (hollow histograms), and cluster members and unclassified objects (shaded), using the membership information presented in the text. (b) As (a), using the statistical field subtraction procedure.

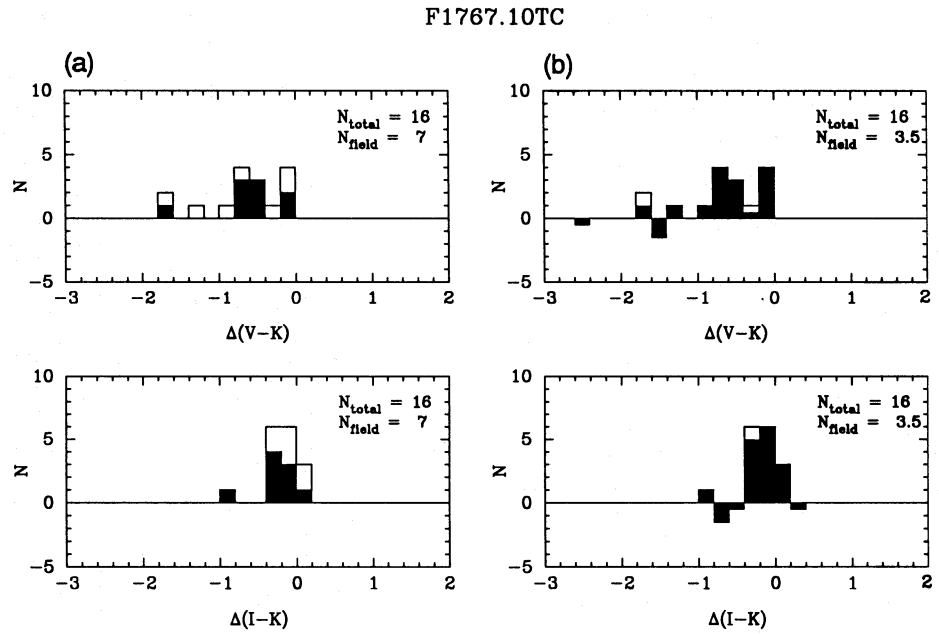

Figure 11. As Fig. 10, for F1767.10TC.

Table 6. Statistical descriptors for the colour distributions.

Colour	$\langle z \rangle$	$C_{BI}^{\dagger}$	$S_{BI}^{\ddagger}$
$(V-K)$	0.56	$-0.38^{+0.05}_{-0.05}$	$0.38^{+0.07}_{-0.07}$
	0.70	$-0.52^{+0.06}_{-0.07}$	$0.43^{+0.05}_{-0.05}$
	0.88	$-1.30^{+0.10}_{-0.09}$	$0.47^{+0.06}_{-0.06}$
$(I-K)$	0.56	$-0.09^{+0.03}_{-0.03}$	$0.27^{+0.06}_{-0.06}$
	0.70	$-0.19^{+0.03}_{-0.03}$	$0.21^{+0.04}_{-0.04}$
	0.88	$-0.39^{+0.10}_{-0.09}$	$0.58^{+0.11}_{-0.11}$

Notes.
†Biweight central location estimator. The errors show 68 per cent ($\sim 1\sigma$) confidence limits.
‡Biweight scale estimator. The errors show 68 per cent ($\sim 1\sigma$) confidence limits.

terms of the epoch and duration of the star formation periods; we recognize that this will be much more difficult and that our conclusions may be non-unique. Furthermore, since the evolutionary predictions remain highly uncertain, especially concerning the bolometric contribution of post-main-sequence stages, we will consider colour changes *relative* to that of a non-evolving model galaxy which is directly comparable with our observed Δ(colour).

Passive evolution, by which we mean the changes arising purely from subsequent movements on the stellar Hertzsprung–Russell (HR) diagram following an initial burst with no further star formation activity, is the minimum possible evolutionary behaviour, although the formation epoch and the duration of the initial burst are variables. Superimposed on that simple evolution may be the effects of more recent star formation, either episodic or declining in intensity from the initial burst. We will consider both cases in the framework of Bruzual's (1983) models. Passive evolution was implemented in Bruzual's *c*-models via a constant star formation rate (SFR) for an initial period τ and zero star formation thereafter. The μ-models extend activity via an SFR that declines exponentially, so that a fraction μ of the galaxy mass is transformed into stars after the first Gyr. The parameter μ is related to the e-folding time τ of the SFR by $\mu \equiv 1 - \exp(-1\ \mathrm{Gyr}/\tau)$. Our calculations were performed with a recent implementation of Bruzual's code, kindly made available by the author, with a solar neighbourhood initial mass function (IMF: Scalo 1986). In relating look-back time and redshift z, we will consider both $q_0 = 0.0$ and $q_0 = 0.5$ for $H_0 = 50$ km s^{-1} Mpc^{-1}. For a given cosmology, the present age of a galaxy is thus determined by the redshift of its formation (z_{for}), corresponding to the epoch at which the major episode of star formation began.

In Fig. 12 we compare the evolutionary predictions of a $\tau = 1$ Gyr *c*-model for various values of q_0 and z_{for} with our observed mean colours as calculated in Section 4.2.4. Fig. 13

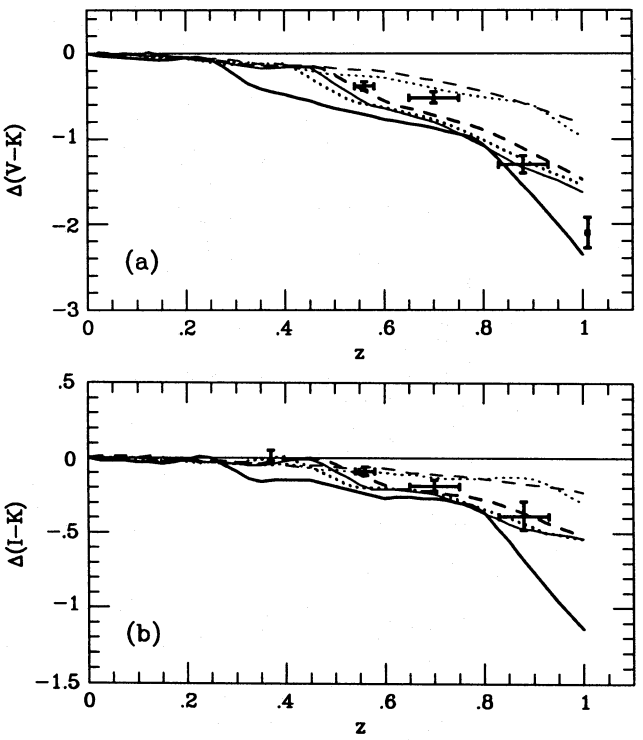

Figure 12. Comparison of the colour distribution properties of our distant clusters binned in three redshift intervals, as described in the text, using Bruzual's (1983) *c*-models ($\tau = 1$ Gyr) with $z_{for} = 2$ (solid lines), $z_{for} = 5$ (dotted lines) and $z_{for} = 10$ (dashed lines), for $q_0 = 0.5$ (thick lines) and $q_0 = 0.0$ (thin lines). Vertical error bars show the $1\,\sigma$ confidence limits for the centre of the field-corrected colour distributions (C_{BI}). Horizontal error bars show the redshift range for each bin. The data for the rich cluster Abell 370 ($z = 0.37$) are also shown in $\Delta(I-K)$. The point at $z = 1.013$ corresponds to the giant elliptical near 3C 245 (see Section 6).

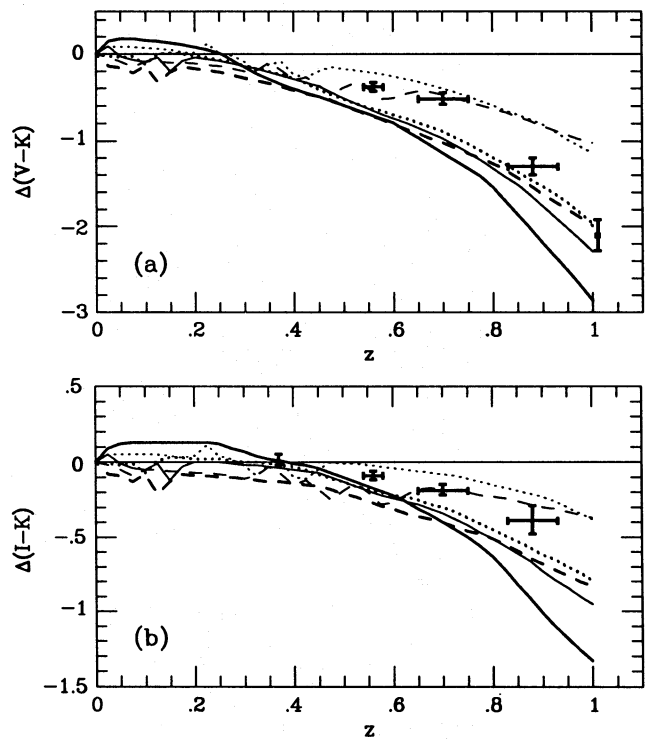

Figure 13. As Fig. 12, for Bruzual's $\mu = 0.5$ model.

shows the same comparison for a $\mu = 0.5$ model (SFR e-folding time = 1.44 Gyr). In the $(I-K)$ figures we have included a data point at $z = 0.37$ derived from the $(685-K)$ colour distribution of Abell 370 cluster members (AES). Strictly speaking, the $(685-K)$ colour distribution does not correspond exactly to $(I-K)$. However, MacLaren et al. (1988) did not detect any evolution in the $(685-862)$ colours of Abell 370 E/S0s, and therefore the $(685-K)$ and $(I-K)$ colours should contain equivalent evolutionary information.

Regardless of how well any particular model fits the observational points, it is clear that the observed colours show significant monotonic trends with redshift that not only delineate the evolution very well, but also *strongly suggest that the galaxies in the various clusters share the same star formation history seen at different stages*. This is an important, purely empirical, conclusion that points to a coeval homogeneous population. While some range in $z_{\rm for}$ is obviously allowed by the data, we point out that the time interval within $2 < z < 5$ is only 1 and 3 Gyr for $q_0 = 0.5$ and 0.0 respectively, and that some degree of coordination between early-type galaxies in different clusters at the same look-back time seems inevitable.

Furthermore, the simple c-models match the trends with redshift very well. At $z \lesssim 0.4$–0.5 little colour evolution is expected and the observations constrain formation to have $z_{\rm for} > 2$. Given the debate about the ages of globular clusters, precision estimates of the ages of cluster ellipticals should obviously be regarded with caution. However, an early epoch for the initial burst is required even if we consider models with a very short time-scale for the initial burst. μ-models with $q_0 = 0.5$ predict too much evolution and generally increase the implied ages, as the models take longer to reach a given red colour today. Thus, regardless of the *form* of the star formation history, our data suggest that the early-type galaxies formed before a redshift $z \simeq 2$.

Unfortunately, an *upper* limit on $z_{\rm for}$ is highly model- and cosmology-dependent. If $q_0 = 0.5$, the models are not very sensitive to this limit because of the short time interval implied before $z = 2$. Here, the c-model is favoured because the μ-models predict evolution which is too strong. For $q_0 = 0.0$, an upper limit of $z_{\rm for} \lesssim 5$ is favoured by the data.

In summary, therefore, the age T of present-day early-type galaxies appears to be $T \gtrsim 10.6$ Gyr if $q_0 = 0.5$, and $13.1 \lesssim T \lesssim 16.3$ Gyr if $q_0 = 0.0$. Of course, we cannot disentangle the effects of galaxy evolution from cosmology. The main results we wish to emphasize are the remarkably uniform evolutionary trends we have found from cluster to cluster, which strongly support a narrow time interval within which the early-type population formed and which, modulo the uncertainties, are consistent with simple evolutionary models where $2 < z_{\rm for} < 5$.

Although we have restricted discussion to Bruzual's (1983) evolutionary models, Arimoto & Yoshii's (1987) model for giant ellipticals predicts colour changes comparable to a c-model with $\tau \simeq 1$ Gyr. The SFR time-scale in both models is similar, and in the latter case the SFR goes abruptly to zero when the superwind phase occurs. The major difference arises in the chemical evolution of the model galaxy (see Aragón-Salamanca 1991 for a detailed comparison of the models). As far as colour–redshift trends are concerned, the conclusions drawn in this section would be the same had we used Arimoto & Yoshii's models.

4.2.6 *Comparison with previous work*

In recent years, extensive photometric and spectroscopic studies have begun for galaxies in intermediate- $(0.35 < z < 0.55)$ and high-redshift clusters by Dressler, Gunn and their collaborators (Dressler & Gunn 1982, 1983, 1988, 1990, 1992; Dressler et al. 1985; Schneider et al. 1986; Dressler 1986, 1987; Gunn & Dressler 1988; Gunn 1989). Much of this work has been concerned with understanding the overabundance of *blue* ('active') cluster galaxies when compared with nearby clusters. In this section we will concentrate on their results for higher redshift ($z \gtrsim 0.5$) clusters, particularly since many of the clusters studied are the same.

Dressler & Gunn (1990) have monitored evolution in the early-type population via the 4000-Å spectral discontinuity or 'break' (D_{4000}), and have claimed to see strong evolution in the sense of much weaker features for their high-redshift galaxies. Hamilton (1985), Dressler & Shectman (1987) and Kimble, Sandage & Davison (1988) showed that the luminosity (and hence metallicity) dependence of D_{4000} is quite weak locally, and thus that the index should reliably measure the location of the main-sequence turn-off for a passively evolving population, or the proportion of hot stars in the case of secondary activity. Aperture effects should similarly not be that important. Dressler & Gunn's data for their highest redshift samples show a shift in the centroid and upper boundary of D_{4000} towards smaller values. The centroid shift, present at $z = 0.35$–0.40, is interpreted as a further manifestation of the Butcher–Oemler effect. The decrease in the upper boundary begins at $z \simeq 0.55$ (0016 + 16), but becomes prominent at $z \gtrsim 0.7$, i.e. a result similar to our own.

There are two difficulties with the D_{4000} studies. First, as we detailed in Section 2.1, since the objects are selected in the Thuan & Gunn (1976) r band, Dressler & Gunn may have missed the oldest, reddest members. Since they typically sampled $\gtrsim 2$ mag fainter than the brightest member, they argued that at least *some* of the reddest objects will be sampled and thus that the shift in the upper boundary of D_{4000}, while statistically weak, cannot be purely due to selection problems. Secondly, the samples are not always complete in apparent magnitude because of geometrical selection effects concerned with the fabrication of multi-aperture masks for the spectroscopy and the absence of features in the spectra. The latter problem is particularly complex, since redshifts will be undetermined for D_{4000}-weak spectra without emission lines whose colours could be intermediate. Thus, while we can qualitatively say that Dressler & Gunn's results agree with our own, the complex nature of the selection criteria makes any quantitative comparison difficult.

We will now argue that, in fact, our colours *are* measuring the D_{4000} index, albeit at low spectral resolution. Fig. 14(a) shows that rest-frame $(U-V)$ colours [corresponding to $\sim(V-I)$ for this redshift range] and D_{4000} are tightly correlated for observed SEDs of different galaxy spectral types and model spectra, and a quadratic fit given by

$$D_{4000} = 1.218 + 0.207\,(U-V)_0 + 0.358\,(U-V)_0^2 \qquad (1)$$

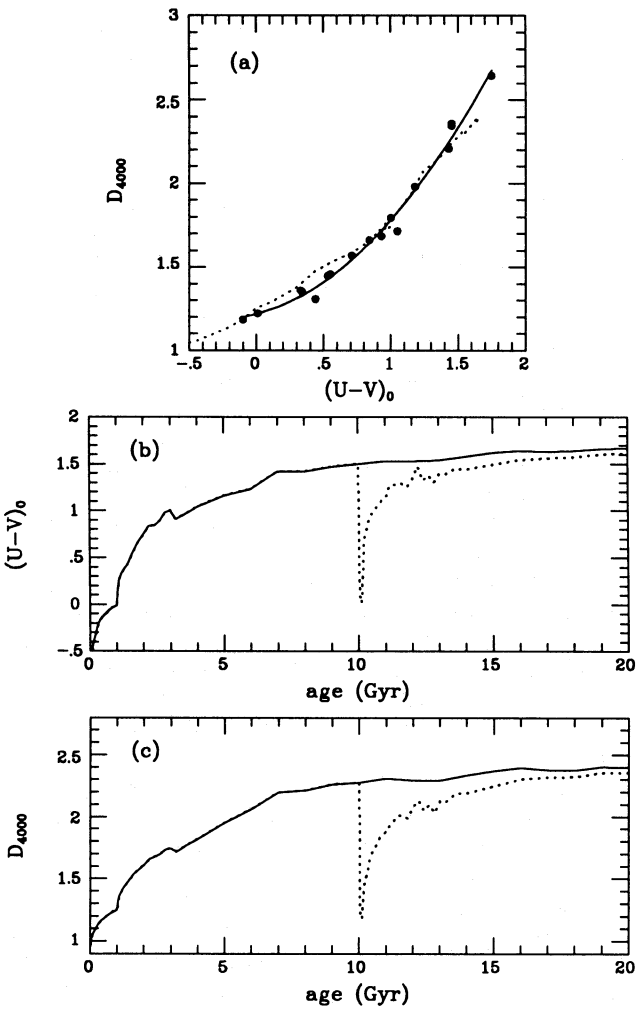

Figure 14. (a) Correlation of D_{4000} versus rest-frame $(U-V)$ for galaxies of different spectral type (filled circles). The solid line is a least-squares second-order polynomial fit to the points. The dotted line shows the same correlation for a passively evolving old stellar population (Bruzual 1983, *c*-model with $\tau = 1$ Gyr). (b) Time evolution of the rest-frame $(U-V)$ colours of a Bruzual (1983) *c*-model with $\tau = 1$ Gyr (solid line), and the same model with a 10 per cent mass burst of star formation happening at an age of 10 Gyr (dotted line). (c) Time evolution of D_{4000} for the same models as presented in (b). Note that when plotting (c) we did not use the correlation plotted in (a), but measured D_{4000} on the model spectra.

(rms = 0.05) can be used to transform one into the other with high accuracy. Figs 14(b) and (c) show that a burst of star formation superimposed on a passively evolving population has a similar effect for both indices. Since the indices are essentially measuring the same thing, their usefulness for monitoring evolution (or measuring changes in the star formation rate) will depend on measurement accuracies, statistical completeness and sample size. In each regard, the photometric approach will be more advantageous. Assuming that the typical D_{4000} errors correspond to the bin size in Dressler & Gunn's histograms (0.1), this equates to a colour change of $\Delta(V-I) \simeq 0.1$ mag which is easily within the capabilities of our photometry.

We thus argue that, while the D_{4000} method has the obvious advantage of clarifying cluster membership, *K*-

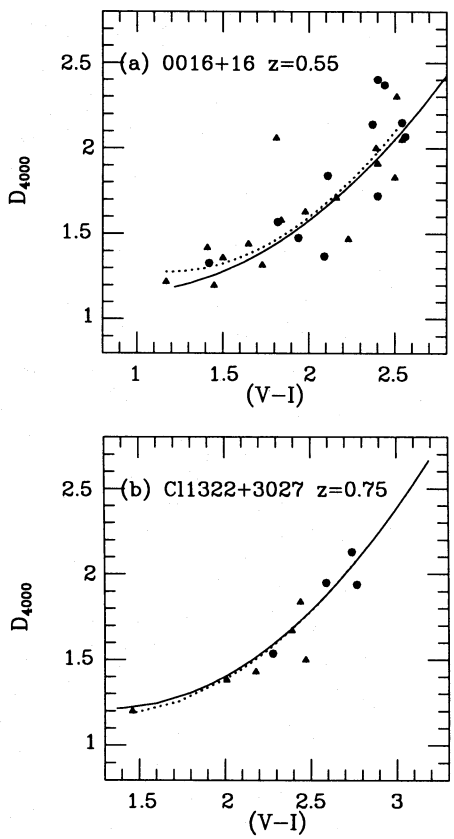

Figure 15. (a) Comparison between D_{4000} from Dressler & Gunn and $(V-I)$ for 0016 + 16. Filled circles: objects in our *K*-selected sample; filled triangles: other cluster members. The solid line represents the calibration presented in Fig. 14(a) at the appropriate redshift, and the dotted line a least-squares fit to the points (excluding the discrepant one). (b) As (a), for Cl1322 + 3027.

selected photometry is less expensive in telescope time and more precise, and larger *complete* samples can be built for a given amount of observing time. Once a cluster has been spectroscopically identified and confirmed, photometric work can substantially enlarge the samples in a reasonable amount of observing time, and important information can be derived from the photometry without the need for further spectroscopy.

A direct comparison between our photometric results and those of Dressler & Gunn is possible because these authors kindly provided their D_{4000} measurements for 0016 + 16 and Cl1322 + 3027. Figs 15(a) and (b) compare D_{4000} and $(V-I)$ colours for the galaxies in common amongst these clusters. Some objects measured by Dressler & Gunn are not in our *K*-selected sample because of the small IRCAM field of view, but optical photometry is available for them, and they have been included. The solid line represents the calibration presented in Fig. 14(a) at the appropriate redshift, and the dotted line is a least-squares second-order fit to the points. The agreement is very good, supporting our previous conclusion that both quantities measure the same physical effect.

4.2.7 *Objects with very red optical–infrared colours*

We now return to the interesting discovery that several objects are found with remarkably red $(I-K)$ colours ($\gtrsim 4.0$)

and a broad range of optical colours (Fig. 8). If these are unrelated field objects, they should be found in deep field surveys. Cowie et al.'s (1992) sample contains only one such object to $K_{\rm lim}=19.5$ mag, although the field is small. In contrast, Elston (1991) claimed to find many red $(R-K)>4.5$ galaxies with $K>17$ mag. Such objects cannot be understood in the framework of current galaxy evolution models, since they are either redder than all cluster galaxies to $z\simeq 1$ or as luminous as radio galaxies at these apparent magnitudes if at higher redshift.

The critical factor in making progress towards an understanding of this phenomenon is the determination of the redshifts of a sample of such sources. Elston, Rieke & Rieke (1989) obtained spectra and *BVRIJHK* photometry for two examples and found that both have $z\simeq 0.8$, with SEDs similar to a current-day elliptical but with a significant ultraviolet excess. Likewise, for the very red galaxies in our sample, $(V-I)$ is anomalously blue for the $(I-K)$ colour, although there is a large variation from object to object. The $(I-K)$ colours alone suggest $z>1$. If the two examples studied by Elston et al. are field galaxies representative of all objects with such colours, the high K luminosity implies a volume density approaching that of L^* galaxies.

A related observation is that of Glazebrook (1991), who found a significant number of less extreme examples [≤ 1 mag redder in $(R-K)$ than non-evolving ellipticals in the redshift range $0.1<z<0.2$] from his K-selected spectroscopic sample. It is not known whether examples are present at higher redshifts. Perhaps these sources need not be at high z and their luminosity is not then unusually high, although their unusually red colours remain unexplained.

AES speculated that current models of galaxy evolution may be inadequate in the near-IR because of their lack of asymptotic giant branch (AGB) stars. Chokshi & Wright (1987) made an attempt to include these late stages of stellar evolution in Bruzual's (1983) models. Depending on the actual contribution of the AGB to the luminosity of the galaxies and its time evolution, their models show that a burst of star formation could make the optical–IR colours of galaxies temporarily *redder*, but probably only by $\simeq 0.2$ mag. However, there are large uncertainties in these models.

None of the above explanations is particularly convincing. If the sources are at high z, as indicated by the very red $(I-K)$ colours, their abundance seems embarrassingly high if they are field galaxies. At lower redshift, the unusually red colours present a serious challenge to evolutionary models. A key discovery is the ultraviolet excess for these sources, found by Elston et al. and confirmed by our $(V-I)$ colours.

5 LUMINOSITY EVOLUTION

We now consider the measurement of the associated *luminosity* evolution for the galaxies in our high-redshift clusters, via K-magnitude–redshift relations for both the brightest cluster galaxies (the Hubble diagram) and the field-subtracted cluster luminosity function.

5.1 The *K* Hubble diagram for the brightest cluster galaxies

The Hubble diagram for brightest cluster galaxies (BCGs) at optical wavelengths was originally introduced as a cosmological test for the determination of q_0 (Peach 1970, 1972; Gunn & Oke 1975; Sandage, Kristian & Westphal 1976; Kristian, Sandage & Westphal 1978; Hoessel 1980; Schneider, Gunn & Hoessel 1983a,b). The 'fully corrected' V Hubble diagram for BCGs has an intrinsic scatter of only 0.28 mag up to $z\sim 0.5$ (Sandage 1988), which may arise as a consequence of the scaling relation between luminosity and surface brightness (Djorgovski et al. 1993). The diagram can be extended to $z=1.8$ using radio galaxies (Djorgovski et al. 1985; Spinrad 1986; Spinrad & Djorgovski 1987). For $z>0.8$, these authors find that the data cannot be fitted by any q_0 value under the assumption of no evolution, whereas a good fit is obtained using a Bruzual (1983) evolving model with $q_0=0.0$ and $H_0=50$. These studies demonstrate, unequivocally, that the optical Hubble diagram could be affected grossly by evolutionary changes, even over modest redshifts, and that conclusions concerning q_0 should not be derived from such diagrams until the evolutionary changes are well understood.

At K, the k-corrections are appreciably smaller than those in B and V, and the evolutionary corrections to $z\leq 1$ should be relatively insensitive to secondary star formation. The passive evolutionary corrections for an old population are also expected to be less, although uncertainties in the behaviour of the giant branch luminosity function may be important.

The Hubble diagram has been extended to the K band mostly for radio galaxies (Grasdalen 1980; Lebofsky 1980; Lilly & Longair 1982, 1984; Lebofsky & Eisenhardt 1986; Lilly 1989a,b), which also prove to have an intrinsic luminosity dispersion of about 0.4 mag for $1<z<2.2$ (Lilly 1989a). Virtually all of the high-redshift data ($z>0.5$) come from radio galaxies and, since it is unclear how representative this class of object is, we have used our sample of high-redshift clusters to study the Hubble diagram for BCGs in the near-IR. To extend the diagram to lower redshifts, we have added data for intermediate-redshift clusters presented in Smail et al. (1993) together with the Coma data of Bower et al. (1992a) and low-redshift data from Peletier et al. (in preparation). K photometry was obtained inside a fixed metric aperture of 50-kpc diameter ($H_0=50$), so that the minimum aperture at high redshift is ~ 5.0 arcsec. Galactic reddening estimates were obtained from the maps of Burstein & Heiles (1982), and k-corrections were determined as before.

Table 7 contains the K magnitudes inside a projected 50 kpc diameter aperture for $q_0=0.0$ and 0.5, and the adopted Galactic absorption and k-corrections for the different clusters. Fig. 16 shows the corrected K-magnitude–redshift diagram for the BCGs for both q_0 values, and the dashed line is a least-squares fit to the data. The formal photometric errors are smaller than the size of the points. The rms scatter about this line is ~ 0.30 mag, which is similar to that found in the optical V diagram to $z\sim 0.5$ after applying the Bautz–Morgan class correction and the richness correction (Sandage 1988). Without these corrections, the V Hubble diagram shows a scatter of 0.35 mag (Sandage & Hardy 1973). We do not have enough information to apply such corrections to our sample, but we can say that the BCGs appear to be better standard candles in K than in V.

The no-evolution predictions (solid lines in Fig. 16a) have been normalized to the data at $z=0.7$ where the density of points is highest. The rms scatter about the no-

Table 7. Photometric data for the K Hubble diagram.

Cluster	z	$K^{50kpc}_{q_0=0.0}$	$K^{50kpc}_{q_0=0.5}$	K_K	A_K
Coma (NGC4889)	0.023	8.82	8.81	−0.07	0.00
Abell 2199 (NGC6166)	0.030	9.42	9.41	−0.08	0.00
Abell 2197 (NGC6173)	0.031	9.46	9.45	−0.08	0.00
Abell 2151 (NGC6034)	0.037	10.39	10.38	−0.10	0.00
Abell 963	0.206	13.21	13.15	−0.40	0.00
Abell 1942	0.224	13.50	13.46	−0.42	0.00
2244-02	0.329	14.85	14.81	−0.50	0.01
Abell 370	0.374	14.53	14.43	−0.52	0.00
0024+16	0.391	14.84	14.71	−0.53	0.01
0016+16	0.546	15.71	15.56	−0.56	0.01
J1888.16CL	0.563	15.75	15.61	−0.56	0.00
Cl0317+1521	0.583	16.57	16.50	−0.56	0.05
F1767.10TC	0.664	16.37	16.24	−0.56	0.00
Cl1322+3029	0.697	16.34	16.16	−0.56	0.00
Cl0020+0407	0.698	16.51	16.46	−0.56	0.01
Cl1322+3027	0.751	16.40	16.22	−0.57	0.00
Cl2155+0334	0.820	16.67	16.57	−0.57	0.02
Cl1603+4313	0.895	17.20	17.06	−0.58	0.00
Cl1603+4329	0.920	17.66	17.44	−0.58	0.00

evolution line is 0.26 mag for $q_0=0.0$ and 0.31 mag for $q_0=0.5$. If we parametrize the K luminosity evolution as $L_K(z)=L_K(0)(1+z)^\gamma$, we obtain $\gamma=-0.09\pm0.3$ and -0.6 ± 0.3 for $q_0=0.0$ and 0.5, respectively. The quoted errors are purely statistical, derived from the least-squares fit. This suggests little evidence for luminosity evolution in the K luminosity of BCGs to the redshifts surveyed here.

We have applied the same analysis to the radio galaxy data of Lilly & Longair (1984), Lilly, Longair & Allington-Smith (1985) and Lilly (1989a), excluding the broad-line radio galaxies, for which there is a strong non-stellar component (cf. Lilly & Longair 1984). We have restricted our study to the $z<1$ range and used the same redshift-related corrections to obtain rest-frame K magnitudes inside a 50 kpc diameter aperture as before. The results are shown in Fig. 16(b). In this case we obtain $\gamma=1.7\pm0.3$ and 1.1 ± 0.3 for $q_0=0.0$ and 0.5, respectively. *This corresponds to radio galaxies being 0.8–1.3 mag brighter at $z\simeq1$ than they are today, in contrast to the results derived for BCGs.* Note also that, for this redshift range, the radio galaxies show an rms scatter of 0.58 mag in absolute K magnitude, in contrast to the results for $1<z<2.2$ (see Lilly 1989a).

In summary, therefore, we find that the radio galaxies do *not* appear to be representative of the giant ellipticals, not being as homogeneous in their evolutionary behaviour and showing somewhat stronger evolutionary trends. This might be taken as evidence that their stellar populations formed over a wider range of epochs, but it could also imply that the BCGs are not a representative subset of normal ellipticals, a point we now address.

5.2 The K luminosity functions

Although BCGs appear to show little evidence for luminosity evolution in the K passband to redshifts $z\simeq1$, it might be argued that they represent a special class of object whose luminosity is affected by other processes, e.g. merging (Hausman & Ostriker 1978), even though their colour evolution does not seem to be any different from the trend shown by other red members. To check this and enlarge the sample, we now consider the evolutionary behaviour of the cluster luminosity functions (LFs).

Since the number of objects per cluster is relatively small, we have combined the data in the three redshift bins defined earlier. As before, we use extinction- and k-corrected K magnitudes inside a fixed 50 kpc diameter projected aperture. Field contamination has been accounted for using the procedures described in Section 4.2. Fig. 17 shows the cumulative LFs for the three redshift bins at two q_0 values. All LFs have been truncated at $M_K=-25.0$ mag for $q_0=0.0$

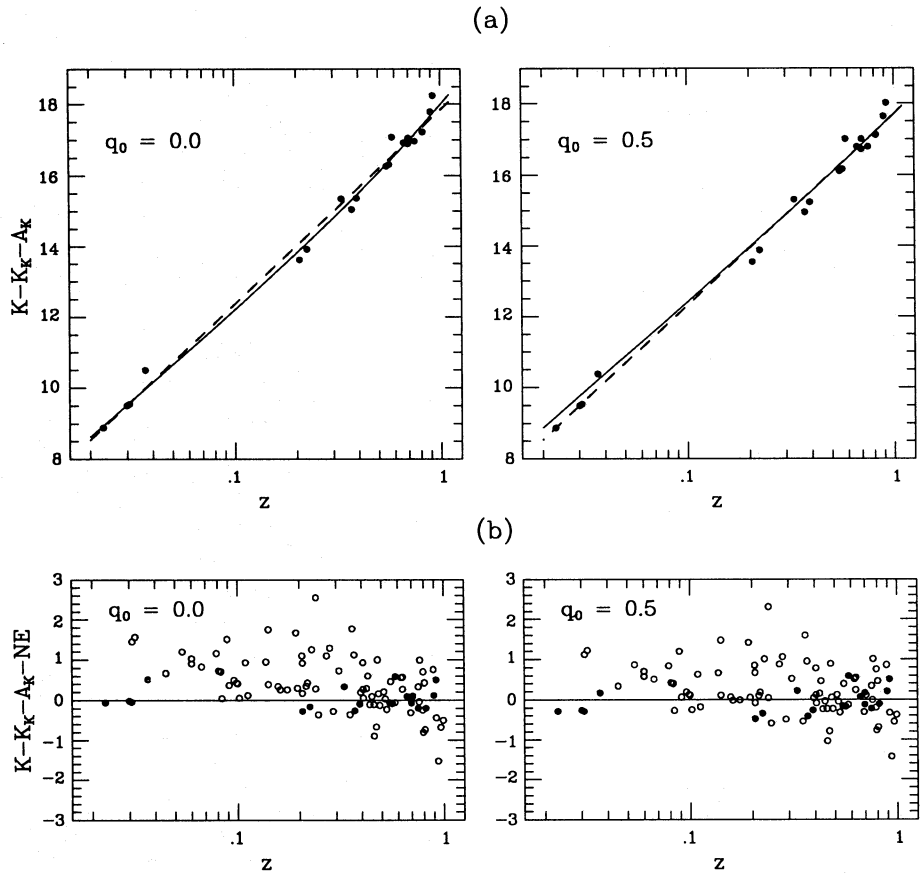

Figure 16. (a) Magnitude–redshift relation (Hubble diagram) for the brightest cluster galaxies in K. The dashed line is a least-squares fit to the data. The solid line shows the no-evolution prediction, normalized to the data at $z=0.7$. The K magnitudes have been measured inside a projected 50 kpc diameter aperture (for two different values of q_0), and the Galactic extinction and k-corrections have been made. (b) Same data after subtracting the no-evolution prediction (filled circles). The open circles correspond to radio galaxies from Lilly et al. (see text for details).

and $M_K=-24.75$ mag for $q_0=0.5$, to ensure that similar luminosity ranges are being sampled for all clusters.

Mobasher, Sharples & Ellis (1993) determined the K-band LF for nearby ($z\lesssim 0.1$) field galaxies. Their best-estimate Schechter function parameters are $M_K^*=-25.1\pm0.3$ and $\alpha=-1.0\pm0.3$. They found no significant differences between the E/S0 and spiral LFs. Minimum-χ^2 fits to our LFs (with fixed $\alpha=-1.0$) yield $M_K^*=-25.2^{+0.3}_{-0.4}$, $-25.3^{+0.4}_{-0.4}$ and $-25.1^{+0.3}_{-0.4}$ for $\langle z\rangle=0.56$, 0.70 and 0.88, respectively,[1] showing no evidence for luminosity evolution. Regrettably, an LF for a K-selected sample of galaxies in a low-redshift cluster is not yet available, so the comparison cannot be extended to $z=0$ for cluster galaxies. Instead, we use the LF of Abell 370 ($z=0.37$), similarly processed, to extend the redshift baseline. For this cluster we obtain $M_K^*=-25.2\pm0.4$.

A Kolmogorov–Smirnov test indicates that the high-redshift LFs are compatible both with one another and also collectively with that of Abell 370. The probability for the null hypothesis (i.e. that all LFs are drawn from a single function) is $\gtrsim 65$ per cent, indicating no K-band luminosity evolution between $z=0.37$ and 0.9, as found for the BCGs. The data rule out luminosity evolution of the magnitude shown by the radio galaxies over this redshift interval (>0.5 mag in K) at a ~ 95 per cent confidence level.

To test if this result is in contradiction with the detected *colour* evolution, we have calculated the luminosity evolution in K implied by the evolutionary models discussed in Section 4.2 that encompass the systematic evolutionary trends seen in our colour data. The comparison is difficult to do with great precision, for a number of reasons. First, since no K-band luminosity functions have yet been determined for low-redshift clusters, the redshift baseline over which luminosity function changes can be consistently measured is small ($0.37<z<0.9$, cf. $0<z<0.9$ for the colour tests). Even if we adopt the local field galaxy luminosity function from Mobasher et al., there is a significant absolute uncertainty in the $z=0$ value of M_K^* (i.e. 0.3 mag). Secondly, the uncertainty in the measured M_K^* at each redshift is sufficiently large that small changes are difficult to discern. Depending on $z_{\rm for}$ and q_0, the models discussed in Section 4.2 predict a brightening of between 0.2 and 0.5 mag in the redshift range for the μ- and c-models respectively. Unfortunately, this is comparable with uncertainties on each measured M_K^* ($\simeq\pm0.4$ mag); as

[1] $q_0=0.5$ is adopted. A 0.16-mag aperture correction has been applied to bring the measures on to the photometric scale of Mobasher et al.

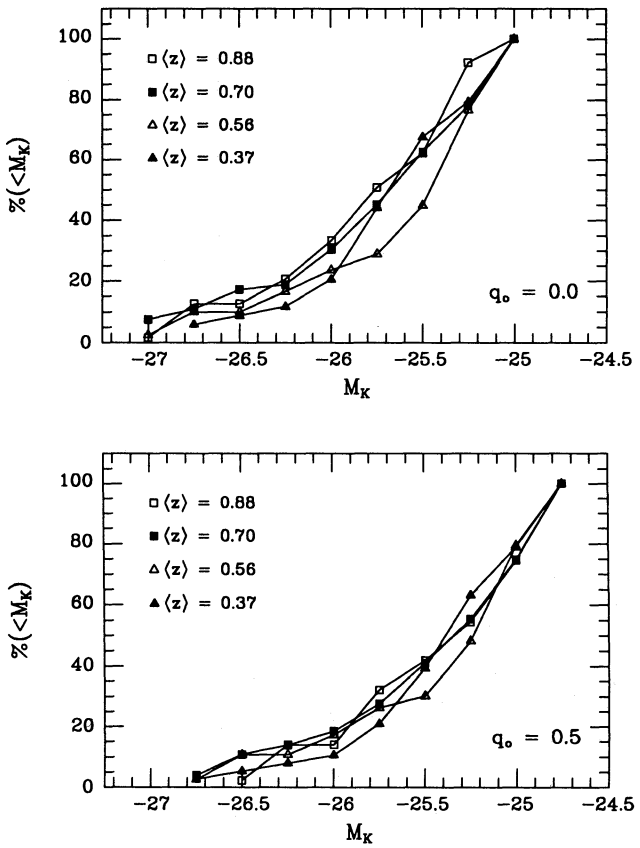

Figure 17. Cumulative K luminosity functions for the galaxies in the high-z cluster sample after field correction. The data are presented in the three redshift bins introduced in previous sections. Two values of q_0 have been considered. The LF of Abell 370 ($z=0.37$) has been plotted for comparison.

such, it is not possible to conclude whether or not our observations are consistent with these predictions. The comparison emphasizes dramatically the greater precision possible with the colour data in constraining the past properties of the cluster members.

6 A RADIO-QUIET GIANT ELLIPTICAL WITH $z=1.013$ NEAR 3C 245

Le Fèvre & Hammer (1992) reported the discovery of what they claim to be the first radio-quiet (down to 3 mJy at 18 cm) elliptical galaxy found at a redshift greater than 1. The galaxy is 2.3 arcsec south-east of the QSO 3C 245, and has $z=1.013$. They concluded that the galaxy is not related to the QSO, but is part of the same cluster or supercluster. The spectrum of the galaxy shows a continuum typical of bright giant ellipticals, with a superimposed emission-line spectrum including [O II] λ3727 Å, which they interpreted as evidence for ongoing star formation. The galaxy, resolved in 0.9 arcsec seeing optical images, has a luminosity profile that fits an $r^{1/4}$ law with $r_e=0.4$ arcsec (3.4 kpc with $H_0=50$ km s^{-1} Mpc^{-1}, $q_0=0.5$).

To test whether the evolutionary trends detected in our cluster galaxies are shared by this high-z elliptical, in 1992 March we obtained a 1440-s K-band IRCAM image (1.2-arcsec pixel mode), and in 1992 April a 1080-s J image (0.6 arcsec pixel^{-1}) was obtained for us in UKIRT service time. In both cases, the 'in field' chopping technique was used and the images were reduced in a standard way. Both images were obtained under good seeing ($\sim$1 arcsec). To obtain the galaxy magnitudes, we subtracted the QSO contribution by following the technique described in Aragón-Salamanca et al. (1993). Essentially, the images were rotated 180°, re-centred and subtracted from the original image (see Aragón-Salamanca et al. for details and a discussion of the uncertainties). We obtained $J_{QSO}=16.11\pm0.03$, $K_{QSO}=15.21\pm0.03$ (total magnitudes), and $J_{gal}=18.5\pm0.1$, $K_{gal}=16.9\pm0.1$ (3.5 arcsec diameter aperture). The aperture size was chosen to match the linear size used at lower redshifts and to minimize the residual contamination from the QSO. Using the V and R photometry from Le Fèvre & Hammer (1992), we obtain $(V-K)=5.56\pm0.18$ and $(R-K)=4.71\pm0.16$ inside the same apertures. The magnitudes that appear in Le Fèvre & Hammer's paper are total, but these authors kindly provided the aperture ones used here. They measured $D_{4000}\simeq1.7$ in the galaxy spectrum. Using the method described in Sction 4.2.6, we obtained $D_{4000}=1.8\pm0.15$ from the measured $(R-J)$, confirming again that equivalent evolutionary information can be obtained from photometry.

A no-evolution prediction was computed as before, and we obtained $\Delta(V-K)\simeq-2.1$, $\Delta(R-K)\simeq-1.1$ and $\Delta(J-K)\simeq-0.5$ relative to a non-evolving elliptical of similar K luminosity (cf. Section 4). Note that the changes in colour detected here are upper limits to the *passive evolution*, since there is clear evidence for *active evolution* in the form of current star formation. The $\Delta(V-K)$ point has been included in Figs 12 and 13. The other colours show a very similar picture when compared with the same set of models. The measured colour evolution for the $z=1.013$ galaxy is marginally larger than that inferred from the passive evolution models favoured by the red cluster galaxies, as expected from the star formation activity present in it. This galaxy is only marginally brighter in K than typical BCGs, despite being $\gtrsim2$ mag brighter than BCGs in the optical, indicating again that the apparently strong luminosity evolution witnessed in the optical is due to changes that involve only a small fraction of the total galaxy mass. The results for this galaxy are, therefore, fully consistent with the trends observed in the high-z clusters.

7 CONCLUSIONS

In this paper we have carried out an optical–IR study of 10 clusters in the redshift range $0.5<z<0.9$. The main conclusions are as follows.

(1) To monitor galaxy evolution in clusters as a function of redshift, it is necessary to select samples independently of the sought-after evolutionary effects. We have shown that near-IR-selected samples should contain a similar proportion of galaxy types at all redshifts, whereas optically selected samples will be increasingly biased towards blue, star-forming objects at high redshift.

(2) Detailed tests in two clusters with extensive spectral and spectrophotometric data demonstrate that field contamination in our cluster samples can be removed by photo-

metric techniques with sufficient accuracy to derive the colour distribution of the cluster members, particularly for the determination of the location of the 'red envelope' at high redshift.

(3) Our field-corrected colour distributions show *systematic* and monotonic evolution as a function of redshift: (i) the *red envelope* moves substantially blueward; at $z \sim 0.9$ there are *no* galaxies as red as present-day ellipticals, indicating significant colour evolution; (ii) the colour distributions at long wavelengths have narrow peaks, and the trends we observe are uniform from cluster to cluster, indicating a remarkably homogeneous population and suggesting a narrow time interval within which the population must have formed, i.e. coevality; and (iii) the tail of blue objects increases with redshift and is more prominent at shorter wavelength colours, as expected for increasing star formation with look-back time.

(4) The colour trends observed for the red envelope can be readily interpreted as the *passive* ageing of an old stellar population that underwent a single burst of star formation before $z = 2$ (and probably after $z = 5$, $H_0 = 50$), in agreement with independent arguments based on precision photometry of local ellipticals.

(5) Superimposed on this passive evolution for the early-type members, we also detect an increase with redshift in the number of blue members. This phenomenon is probably an extension to higher redshift of the Butcher–Oemler effect, whose physical origin will be addressed in subsequent papers.

(6) We demonstrate that, within the redshift range studied here, our $(V-I)$ photometry is essentially measuring the D_{4000} spectral discontinuity, but with better precision and for more complete samples than have been available hitherto. A one-to-one comparison of D_{4000} and $(V-I)$ for two clusters from the survey of Dressler & Gunn (1990) confirms the validity of our approach.

(7) The K-magnitude–redshift relation (Hubble diagram) for the brightest cluster members is very tight. Without applying richness and Bautz–Morgan corrections, the scatter to $z \simeq 0.9$ is $\sigma_K = 0.30$ mag, cf. $\sigma_V = 0.35$ mag to $z \simeq 0.5$. The scatter is significantly smaller than for radio galaxies, where $\sigma_K \simeq 0.58$ mag to $z \simeq 1$.

(8) We do not detect significant amounts of K luminosity evolution for the BCGs or the cluster luminosity functions between $0.37 < z < 0.9$, in contrast to the results obtained for radio galaxies. This suggests that the evolutionary properties of very high-redshift radio galaxies may *not* be representative of those for early-type galaxies. Our upper limits on the K luminosity evolution are compatible with those implied from our detected colour evolution, reinforcing the sensitivity of our method over and above that possible from the Hubble diagram alone.

ACKNOWLEDGMENTS

We thank PATT for generous and continuing allocations of time on the UK Infrared Telescope over several years, the UKIRT telescope operators for their dedicated support and good humour, and Mark Casali for help with IRCAM reductions and software. We also thank staff at La Palma and the Anglo–Australian Telescope for their efficient service observing programme, which provided virtually all of the optical data. Many of the data were taken with the co-operation and help of Ian Smail, to whom we are very grateful. We acknowledge useful discussions with Richard Bower, Alan Dressler, Mike Edmunds, Jim Gunn, John Lucey, Gus Oemler, Alvio Renzini and Simon White. We thank Alan Dressler for his generosity in sending pre-publication data on two clusters and for his interest in this project. AAS acknowledges financial support from the Physics Department of Durham University and the Spanish 'Ministerio de Educación y Ciencia'. RSE was supported by SERC for part of this work. WJC acknowledges the financial support of the Australian Research Council.

NOTE ADDED IN PROOF

After this paper was submitted for publication, Dunlop & Peacock (1993) presented evidence indicating that a significant fraction of the extended optical/infrared emission in powerful 3CR radio galaxies is directly related to the presence of an AGN. They suggest that this could account for the 1-mag brightening seen to $z \sim 1$ by Lilly and co-workers and, therefore, that powerful 3CR radio galaxies may not be representative giant ellipticals, as we suggest. However, Dunlop & Peacock also find that this effect is largely confined to the top decade of radio power, and that less extreme radio galaxies may still be useful as probes of elliptical galaxy evolution. Weaker radio galaxies show a low degree of star-forming activity at $z = 1$, in agreement with our results.

REFERENCES

Allington-Smith J. R., Ellis R. S., Zirbel E. L., Oemler A., 1993, ApJ, 404, 521
Aragón-Salamanca A., 1991, PhD thesis, Durham University
Aragón-Salamanca A., Ellis R. S., Sharples R. M., 1991, MNRAS, 248, 128 (AES)
Aragón-Salamanca A., Ellis R. S., Schwartzenberg J.-M., Bergeron J., 1993, ApJ, submitted
Arimoto N., Yoshii Y., 1986, A&A, 164, 260
Arimoto N., Yoshii Y., 1987, A&A, 173, 23
Beers T. C., Flynn K., Gebhard K., 1990, AJ, 100, 32
Bower R. G., Lucey J. R., Ellis R. S., 1992a, MNRAS, 254, 589
Bower R. G., Lucey J. R., Ellis R. S., 1992b, MNRAS, 254, 601 (BLE)
Broadhurst T. J., Ellis R. S., Glazebrook K., 1992, Nat, 355, 55
Bruzual G., 1983, ApJ, 273, 105
Bruzual G., Kron R. G., 1980, ApJ, 241, 25
Burstein D., Heiles C., 1982, AJ, 87, 1165
Butcher H., Oemler A., 1978, ApJ, 219, 18
Butcher H., Oemler A., 1984, ApJ, 285, 426
Chambers K. C., Charlot S., 1990, ApJ, 384, L1
Charlot S., Bruzual A. G., 1991, ApJ, 367, 126
Chokshi A., Wright E. L., 1987, ApJ, 319, 44
Colless M., Ellis R. S., Taylor K., Hook R. N., 1990, MNRAS, 224, 408
Colless M., Ellis R. S., Broadhurst T. J., Taylor K., Peterson B. A., 1993, MNRAS, 261, 19
Couch W. J., Newell E. B., 1984, ApJS, 56, 143
Couch W. J., Sharples R. M., 1987, MNRAS, 229, 423
Couch W. J., Ellis R. S., Godwin J., Carter D., 1983, MNRAS, 205, 1287
Couch W. J., Shanks T., Pence W. D., 1985, MNRAS, 213, 215
Couch W. J., Ellis R. S., Malin D. F., MacLaren I., 1991, MNRAS, 249, 606 (CEMM)

Cowie L. L., Gardner J. P., Lilly S. J., McLean I., 1990, ApJ, 360, L1
Cowie L. L., Songaila A., Hu E. M., 1991, Nat, 354, 460
Cowie L. L., Gardner J. P., Wainscoat R. J., Hodapp K. W., 1992, preprint
Djorgovski S., Spinrad H., Maar J., 1985, in Nieto J. L., ed., Lect. Notes Phys. Vol. 232, New Aspects of Galaxy Photometry. Springer-Verlag, Berlin, p. 193
Djorgovski S., de Carvalho R., Shlosman I., Schombert J., 1993, in Busarello G., Longo G., Capaccioli M., eds, Morphological and Physical Classification of Galaxies. Springer-Verlag, Berlin, in press
Dressler A., 1986, in Chiosi C., Renzini A., eds, Spectral Evolution of Galaxies. Reidel, Dordrecht, p. 375
Dressler A., 1987, in Faber S. M., ed., Nearly Normal Galaxies: from the Planck Time to the Present. Springer-Verlag, New York, p. 265
Dressler A., Gunn J. E., 1982, ApJ, 263, 533
Dressler A., Gunn J. E., 1983, ApJ, 270, 7
Dressler A., Gunn J. E., 1988, in Audouze J., Pelletan, M.-C., Szalay A., eds, Large Scale Structure of the Universe. Kluwer, Dordrecht, p. 311
Dressler A., Gunn J. E., 1990, in Kron R. G., ed., ASP Conf. Ser. Vol. 10, Evolution of the Universe of Galaxies: Edwin Hubble Centennial Symposium. Astron. Soc. Pac., San Francisco, p. 200
Dressler A., Gunn J. E., 1992, ApJS, 78, 1
Dressler A., Shectman S. A., 1987, AJ, 94, 899
Dressler A., Gunn J. E., Schneider D. P., 1985, ApJ, 294, 70
Dunlop J. S., Peacock J. A., 1993, MNRAS, in press
Elias J. H., Frogel J. A., Mathews K., Neugebauer G., 1982, AJ, 87, 1029
Ellis R. S., 1990, in Kron R. G., ed., ASP Conf. Ser. Vol. 10, Evolution of the Universe of Galaxies: Edwin Hubble Centennial Symposium. Astron. Soc. Pac., San Francisco, p. 248
Ellis R. S., Couch W. J., MacLaren I., Koo D. C., 1985, MNRAS, 217, 239
Elston R. S., 1991, in Elston R., ed., ASP Conf. Ser. Vol. 14, Astrophysics with Infrared Arrays. Astron. Soc. Pac., San Francisco, p. 3
Elston R. S., Rieke M. J., Rieke G. H., 1989, ApJ, 341, 80
Glazebrook K., 1991, PhD thesis, University of Edinburgh
Graham J. A., 1981, PASP, 94, 244
Grasdalen G. L., 1980, in Abell G. O., Peebles P. J. E., eds, Proc. IAU Symp. 92, Objects of High Redshift. Reidel, Dordrecht, p. 269
Gunn J. E., 1989, in Frenk C. S., Ellis R. S., Shanks T., Heavens A. F., Peacock J. A., eds, The Epoch of Galaxy Formation. Kluwer, Dordrecht, p. 167
Gunn J. E., Dressler A., 1988, in Renzini A., Kron R. G., eds, Towards Understanding Galaxies at High Redshift. Kluwer, Dordrecht, p. 227
Gunn J. E., Oke J. B., 1975, ApJ, 195, 255
Gunn J. E., Hoessel J. G., Oke J. B., 1986, ApJ, 306, 30 (GHO)
Hamilton D., 1985, ApJ, 297, 371
Hausman M. A., Ostriker J. P., 1978, ApJ, 224, 320
Hoessel J. G., 1980, ApJ, 241, 493
Johnson H. L., 1966, ARA&A, 4, 193
Kimble R. A., Sandage A., Davison A. F., 1988, preprint
Koo D. C., 1981, ApJ, 251, L75
Koo D. C., 1986, ApJ, 311, 651
Koornneef J., 1983, A&A, 128, 84
Kristian J., Sandage A., Westphal J. A., 1978, ApJ, 221, 383
Landolt A. U., 1983, AJ, 88, 439
Lavery R. J., Henry J. P., 1986, ApJ, 304, L5
Lavery R. J., Henry J. P., 1988, ApJ, 330, 596
Lebofsky M. J., 1980, in Abell G. O., Peebles P. J. E., eds, Proc. IAU Symp. 92, Objects of High Redshift. Reidel, Dordrecht, p. 257
Lebofsky M. J., Eisenhardt P. R. M., 1986, ApJ, 300, 151
Le Fèvre O., Hammer F., 1992, A&A, 254, L29
Lilly S. J., 1988, ApJ, 333, 161
Lilly S. J., 1989a, ApJ, 340, 77
Lilly S. J., 1989b, in Frenk C. S., Ellis R. S., Shanks T., Heavens A. F., Peacock J. A., eds, The Epoch of Galaxy Formation. Kluwer, Dordrecht, p. 63
Lilly S. J., Longair M. S., 1982, MNRAS, 199, 1053
Lilly S. J., Longair M. S., 1984, MNRAS, 211, 833
Lilly S. J., Longair M. S., Allington-Smith J. R., 1985, MNRAS, 215, 37
Lilly S. J., Cowie L. L., Gardner J. P., 1991, ApJ, 369, 79
MacLaren I., Ellis R. S., Couch W. J., 1988, MNRAS, 230, 249
McLean I. S., Chuter T. C., MacCaughrean M. J., Rayner J. T., 1986, Proc. SPIE, 627, 430
Mathis J. S., 1990, ARA&A, 28, 37
Mobasher B., Sharples R. M., Ellis R. S., 1993, MNRAS, in press
O'Connell R., 1988, in Renzini A., Kron R. G., eds, Towards Understanding Galaxies at High Redshift. Kluwer, Dordrecht, p. 177
Oemler A., 1992, in Fabian A. C., ed., Clusters and Superclusters of Galaxies. Kluwer, Dordrecht, p. 29
Peach J. V., 1970, ApJ, 159, 753
Peach J. V., 1972, in Evans D. S., ed., External Galaxies and Quasi-Stellar Objects. Proc. IAU Symp. 44, Reidel, Dordrecht, p. 314
Peletier R. F., Davies R. L., Illingworth G. D., Davis L. E., Cawson M., 1990, A&A, 100, 1091
Persson S. E., Frogel J. A., Aaronson M., 1979, ApJS, 39, 61
Sandage A., 1988, ARA&A, 26, 561
Sandage A., Hardy E., 1973, ApJ, 183, 743
Sandage A., Visvanathan N., 1978, ApJ, 223, 707
Sandage A., Kristian J., Westphal J. A., 1976, ApJ, 205, 688
Savage B. D., Mathis J. S., 1979, ARA&A, 17, 73
Scalo J. M., 1986, Fundam. Cosmic Phys., 11, 1
Scarrott S. M., Rolph C. D., Tadhunter C. N., 1990, MNRAS, 243, 5P
Schneider D. P., Gunn J. E., Hoessel J. G., 1983a, ApJ, 264, 337
Schneider D. P., Gunn J. E., Hoessel J. G., 1983b, ApJ, 268, 476
Smail I., Ellis R. S., Aragón-Salamanca A., Soucail G., Mellier Y., Giraud E., 1993, MNRAS, in press
Spinrad H., 1980, in Abell G. O., Peebles P. J. E., eds, Proc. IAU Symp. 124, Objects of High Redshift. Reidel, Dordrecht, p. 39
Spinrad H., 1986, PASP, 98, 269
Spinrad H., Djorgovski S., 1987, in Hewitt A., Burbidge G., Fang L.-Z., eds, Proc. IAU Symp. 124, Observational Cosmology. Reidel, Dordrecht, p. 129
Thuan T. X., Gunn J. E., 1976, PASP, 88, 543
Tinsley B. M., 1972, ApJ, 20, 283
Tinsley B. M., Gunn J. E., 1976, ApJ, 203, 52
UKIRT Observer's Manual, 1989, UK Infrared Telescope Support Unit, Royal Observatory, Edinburgh
UKIRT Observer's Manual, 1991, UK Infrared Telescope Support Unit, Royal Observatory, Edinburgh
Yoshii Y., Takahara F., 1988, ApJ, 326, 1